Laser Treatment of Hemangiomas Using Spectroscopic Feedback: The "Smart Scalpel"

by

Elizabeth Lynn Sebern

S.B., Mechanical Engineering (1997)

Massachusetts Institute of Technology

Submitted to the Department of Mechanical Engineering
in Partial Fulfillment of the Requirements for the Degree of
Master of Science in Mechanical Engineering

at the

MASSACHUSETTS INSTITUTE OF TECHNOLOGY

June 1999

Signature of Author .....
Department of Mechanical Engineering
May 7, 1999

Certified by .....
Ian W. Hunter
Hatsopoulos Professor of Mechanical Engineering
Thesis Supervisor

Accepted by .....
Ain A. Sonin
Chairman, Department Committee on Graduate Students

Laser Treatment of Hemangiomas Using Spectroscopic Feedback: The "Smart Scalpel"

by

Elizabeth Lynn Sebern

Submitted to the Department of Mechanical Engineering on May 7, 1999
in Partial Fulfillment of the Requirements for the Degree of
Master of Science in Mechanical Engineering

Abstract

While feedback control is widespread throughout many engineering fields, surgical instruments with embedded feedback control systems are uncommon. To improve the effectiveness of microsurgical techniques, we are presently developing a semi-autonomous robotic surgical tool (called the "Smart Scalpel") as an alternative approach to treatment of skin hemangiomas like nevus flammus (port wine stain or PWS). Current PWS phototherapy relies on selective absorption of optical radiation by the ectactic blood vessels in a PWS resulting in thermally mediated vessel necrosis. Although shown to be effective, heating of the surrounding tissue by photon absorption results in unacceptable collateral damage. The Smart Scalpel approach employs optical reflectance spectroscopy to selectively target blood vessels in a PWS for heating with a focused laser beam. Collateral damage to adjacent tissue is substantially minimized and continuous imaging throughout the procedure allows modification of the delivered therapy to optimize therapeutic outcomes. Our work reported here involves optical system design and construction, initial quantification of imaging system resolution and contrast, and preliminary verification of the imaging and targeting strategies.

Thesis Supervisor: Ian Hunter

Title: Hatsopoulos Professor of Mechanical Engineering

Table of Contents

Table of Figures

Acknowledgements

I wish to acknowledge the many people who have challenged and supported me throughout my graduate studies during the past two years.

First, thank you Professor Ian Hunter for offering me the opportunity to be a part of your laboratory. I have been most impressed with your ability to become involved with exciting, interdisciplinary projects, as well as your creative ideas for solving these engineering problems. I remember speaking with you during the spring of my senior year, when I was deciding where to do my graduate research. You expressed your confidence that completing a Masters degree in your lab would set me up well for whatever future path I might choose to take. This couldn't have been more true. Through my interactions with you and other members of the lab, I have felt like a sponge, soaking up creative ideas and knowledge from a range of disciplines and perspectives.

Next, I must recognize Dr. Colin Brenan, my excellent mentor over the past two years. I came in with a mechanical engineering background and limited exposure to the optics and programming skills required for this project. I leave with a broader understanding of these and many other areas. Thank you for patiently teaching and directing me through the process of designing and developing this complex, multifaceted system. Also, thank you for your encouragement of my participation in academic conferences.

Thank you Dr. Tanya Kanigan for mentioning, back in the fall of 1997, the Smart Scalpel project as a possibility for my Masters thesis. The practical and clinical aspects for the project fit well with my interests. Also, I must thank you for all your support and the fun times we've had. You are a dear friend, and I'll miss you terribly next year.

Okay, now I should acknowledge the soon-to-be Drs. John Madden, Peter Madden, and James Tangorra. You three really helped orient me into the lab that first term, and it was always nice to see your smiling faces all those long days and late nights in lab. Also, I must recognize Matthew Graham and Robert David for putting up with all those dark days in the cave of the spectroscopy lab.

Finally, I'd like to thank my friend, Kelly Hetherington (I don't know what I'll do without you next year!) and my parents, Marge and Mark Sebern, for your generous support through the stress and excitement of this graduate school experience.

Now that my thesis is about to be signed and handed in, I realize my MIT tenure is drawing to a close. MIT has been an amazing place that has helped me develop into a confident engineer and person. I feel well-prepared and excited for the path that lies ahead.

Now let's go see about that **yard** . . . .

Chapter One

Background and Motivation

Closed-loop feedback control is widespread throughout many engineering fields, such as manufacturing, robotics, and in other human-machine interfaces. A general characteristic of any feedback control scheme is the comparison of the output of a physical system with its input to generate an error signal. The error signal, in turn, modifies the system to minimize the difference between input and output [Dorf and Bishop, 1995]. Feedback control, therefore, maintains system equilibrium (with respect to its input) by quickly compensating for changes in the physical system or perturbations imposed on it by the external environment.

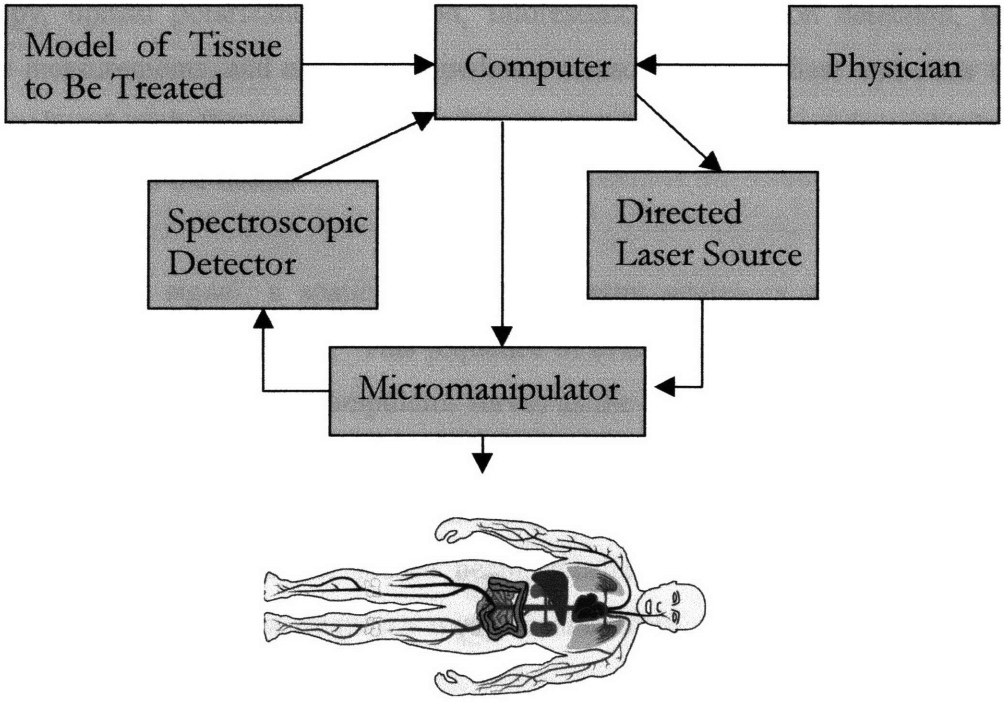

Figure 1: Schematic illustration of the "Smart Scalpel."

An interesting potential application of feedback control is in the field of microsurgery. Many microsurgical procedures require a high degree of physical dexterity, accuracy, and control, which may degrade rapidly with physician fatigue. This problem could be partially alleviated through inclusion of low-level decision-making embedded in a microsurgical tool to aid in tissue

location and removal. Our embodiment of this concept is a device we call the Smart Scalpel (Figure 1).

Implementation of the Smart Scalpel concept is quite general in both measurement and intervention techniques. Physical properties of normal and diseased or damaged tissue as well as expert knowledge from the physician operator are inputs to a computer model describing the attributes of healthy tissue versus the diseased or damaged tissue to be excised. Histochemical and morphological tissue properties non-invasively measured in real-time provide the feedback needed to selectively identify tissue targets by comparison with the tissue computer model. Techniques to measure one or more physical attributes of the tissue include optical reflectance spectroscopy, magnetic resonance imaging, fluorescence optical spectroscopy, Raman spectroscopy, optical polarization detection, fluorescence polarization detection, mechanical impedance measurements, and electrical impedance measurements. These and other techniques may be employed with the goal of delineating among tissue types based on the information acquired directly from the tissue.

Using this feedback signal, a spatially localized energy source is applied for removal or modification of the specified tissue. This sequence of events repeats itself until all the targeted tissue has been treated. A micromanipulator serves as the interface between the patient and the Smart Scalpel, providing a means to extract information about the tissue state and direct the therapeutic energy source to the appropriate targets. Examples of directed energy sources include: photon beam, electron or proton beam, localized electrical field, directed acoustic energy, and inertial cutting (low frequency mechanical energy).

The many desirable attributes of the Smart Scalpel have the potential to not only improve performance in current microsurgical procedures but also facilitate the development of new treatments not yet feasible with existing technology. The accuracy and reliability of present-day procedures may be enhanced and collateral damage minimized through quantitative, rapid, on-line assessment of the procedure efficacy. This system of real-time feedback has great potential to increase patient comfort, shorten patient recovery times, and decrease the overall cost per

procedure. Additionally, the Smart Scalpel is amenable to integration into a tele-operation system for remote surgery.

There are many possible medical applications for the Smart Scalpel including:

- Removal of port wine stains (PWS) and other hemangiomas;
- Treatment of varicose veins;
- Permanent or semi-permanent hair removal;
- Destruction of cancerous and pre-cancerous tumors;
- Photorefractive keratectomy; and
- Neurosurgery.

Attempts have been made to utilize robotics and/or feedback control to enhance the clinical outcomes of some laser-based medical procedures, including: port wine stain removal [Mordon *et al.,* 1993], laser photocoagulation of the retina [Inderfurth *et al.*, 1994], laser-assisted vascular welding [Stewart *et al.,* 1996], and laser incisions [Reinisch, Mendenhall and Ossoff, 1997]. Developments in automated PWS treatment will be discussed in the following section.

Optical reflectance measurements have been employed as a feedback signal to control laser photocoagulation of the retina. Photocoagulation of the retina may serve several surgical purposes, such as: clearing obstructions caused by pathological blood vessels, stimulation of retinal pigment epithelium proliferation, destruction of oxygen consuming photoreceptor cells, or the formation of chorio-retinal adhesions. As the laser heats the retina, once there is enough energy per unit volume deposited for the coagulation process, the protein begins to denature. As this protein denatures the retinal tissue scatters more light, making it appear whitish. In these treatments, feedback-controlled photocoagulation, based on the increase in back-scattered laser light of the retinal reflectance signal, limits the complications of over- or under-treatment. The reflectance of the coagulation beam is monitored in a confocal arrangement to improve discrimination [Inderfurth *et al.*, 1994].

In laser assisted vascular welding, a system utilizing real-time feedback control based on skin temperature has been developed. Lasers are advantageous in minimally invasive procedures, where the conventional suture-tying technique is extremely difficult. Potential benefits for feedback control scheme include: shorter operative times, reduced foreign-body reaction, and reduced bleeding. Tissue parameters that could provide diagnostic information about the tissue weld include native autofluorescence, optical birefringence, and tissue temperature. One instrument [Stewart *et al.*, 1996] employs a laser/infrared thermometer system to control the surface temperature of the weld within ± 2 °C by modifying the laser current every 5 ms based on the difference between the actual and desired temperatures. Both the weld success rate and the pressures required to burst the vessel weld were significantly higher for the closed loop welds controlled near the optimal temperature than for welds created without feedback control.

A system to improve the precision of laser incisions uses real-time closed loop feedback to correct for low frequency patient movements resulting from respiration and blood flow [Reinisch, Mendenhall and Ossoff, 1997]. Before treatment, the tissue is tagged with one or more pins with green heads. The movement of these pins is then tracked for a short time (~30 s), the x-y position of the pins are computed and record by the computer, and then the Maximum Entropy Method is used to predict future motion. This method can be used to track low-frequency movements, such as breathing, pulse, and heart beat. However, the video acquisition time (16 ms) of the system is to slow to track motions such as spasmodic tremors or motions of the eye. The resulting system has occasional false predictions, but the motion compensation gives a better incision than manual surgical methods, as the system effectively subtracts away nearly all patient motions. Disadvantages of this system are that it is highly invasive and has low accuracy, both spatially and temporally.

These instruments are similar to the Smart Scalpel in that the feedback signal is a direct measurement of tissue properties. However, in the treatment of PWS, the Smart Scalpel system aims for much greater spatial resolution and bandwidth than these instruments. Great resolution and bandwidth are required to treat tissue structures of ~50 um dimension in a 10 mm by 10mm region of skin within ~50 ms to eliminate problems associated with relative motion between the instrument and the patient.

Chapter Two

Application to Nevus Flammus (Port Wine Stains)

A first demonstration of the Smart Scalpel is the removal of nevus flammus (port wine stain or PWS) and other hemangiomas. PWS is a congenital, vascular malformation of the dermis, which is estimated to occur in five children per thousand births [Mulliken and Young, 1988]. On the macroscopic scale, a port wine stain appears pink, red, or purple, in which lesion color correlates with vessel diameter. Pink lesions have a mean vessel diameter of 16 μm while purple lesions have a mean diameter of 51 μm. Also, pink and purple lesions have significantly deeper blood vessels than red ones [Fiskerstrand *et al.*, 1997]. Vessel number is highest in the immediate subepidermal layer and then rapidly diminishes with depth into the subdermal layers; mean vessel depth are found to be 460 ± 170 μm [Barsky *et al.*, 1980].

2.1 Current clinical practice

Current PWS therapy involves the illumination of ~10 mm diameter regions of skin with the output from a pulsed dye laser (t_{pulse} ~ 0.4 ms) having a fluence level between 40 - 80 kJ/m^2 at a wavelength coincident with a oxyhemoglobin absorption band (typically 577 nm) [Anderson, 1996]. Selective absorption of the laser energy by the blood results in thermal necrosis of blood vessels. Over time the body absorbs these vessels, and the PWS fades or completely disappears. In practice, the collateral damage to the surrounding tissue results in pain for the patient and tissue scarring. The procedure is slow (>1 hour/session × >8 session/treatment) and treatment response is poor when blood vessels are deep and relatively small. Most important in the context of the Smart Scalpel is that, aside from PWS appearance, no feedback is generated to assess treatment efficacy or appropriateness of the photon dosage.

2.2 Dynamic epidermal cooling using cryogens

Because current laser treatments significantly heat the epidermis and the dermal blood vessels, efforts are being made to cool the epidermis using cryogen spray cooling (CSC). CSC is currently being experimented with in tissue phantoms [Torres *et al.*, 1999], animal models [Anvari *et al.*, 1997], and in pre-clinical settings [Nelson *et al.*, 1995], as a means to protect the

epidermis from nonspecific thermal injury, while heating blood vessels in the dermal layer. Sustained cryogen cooling creates a near-linear steady state temperature distribution that cools both the epidermis and the core temperature of the PWS vessels. Therefore, any epidermal cooling is offset by the need for increased energy required for blood vessel photothermolysis. With dynamic cryogen cooling taking place on the order of tens of milliseconds, the spatial distribution of the cooling remains localized in the epidermis, leaving the temperature of deeper PWS blood vessels unchanged. This dynamic cooling reduced the level of patient pain and discomfort, decreased hypertrophic scarring and, at the 6-month treatment follow-up, showed significant blanching (comparable with the uncooled controls) on all cooled test sites[Nelson *et al.*, 1996]. However, while dynamic CSC is promising for limiting damage to the epidermis, collateral damage still occurs in the dermal layer.

2.3 Attempts at automated port wine stain removal

In port wine stain removal, automatic scanners have been developed to achieve more uniform laser dosage than manual techniques can accomplish. This greater uniformity in energy delivery is expected to reduce poor clinical outcomes, such as hypertrophic scarring, inhomogeneity of blanching, and poor reproducibility from one operator to another, as well as to reduce the tediousness of the physician sequentially scanning the laser beam throughout the PWS. Two categories of automated treatment devices have been developed: scanners and automated handpieces. In the first category, the two systems developed are the Multiscan [Laffitte *et al.*, 1992] and the Scanall [Smithies *et al.*, 1991]. These instruments automatically scan the laser spot over the PWS. Multiscan produces a 5 mm spot diameter, and the Scanall system uses a 0.5 mm spot diameter. The velocity of scanning (50 to 300 mm/s) is adjusted to provide the appropriate incident fluence. Both scanners work without contacting the skin, and Scanall uses a video camera to obtain an image of the lesion, and this image is mapped to the computer memory to limit the laser treatment to the PWS.

Hexascan [McDaniel and Mordon, 1990] and CC-scan [Chambers, Clark and Bainbridge, 1990] are automated handpieces controlled by a scanner mechanism composed of two stepper motors. The motors are controlled by a microprocessor so they can be programmed to scan the laser across the treatment area in a variety of predefined patterns. The Hexascan handpiece contains a

power meter and a shutter to ensure that there is ample cooling between two adjacent spots. Comparing the results between the conventional "free hand point-by-point" technique and the Hexascan automated handpiece reveals a factor of two increase in the percentage of good clinical results. Treatment duration was reduced to 20% of the point-by-point technique, and a drastic reduction in hypertrophic scarring was observed [Mordon *et al.*, 1993].

In all four automated scanning systems the goal is greater uniformity in laser delivery than manual techniques. Still, laser energy is delivered to the entire region of the PWS. No effort is made to discriminate between blood vessels, which need to be treated, and the surrounding tissue, where unnecessary collateral damage occurs.

2.4 Smart Scalpel approach

The Smart Scalpel is a radical departure from these automated approaches. Rather than servo-control based on the laser power delivered to the tissue, we are using the blood vessel reflectance signal to first identify the blood vessels to be treated and also monitor this signal throughout the treatment to optimally heat and photocoagulate the blood vessels. The Smart Scalpel approach to PWS treatment requires, first, locating the blood vessels within a volume of PWS and, second, illuminating selected blood vessels with light from a focused laser beam for a time sufficient to increase the local vessel temperature to cause permanent physical damage. Major design components of the PWS Smart Scalpel are (1) a non-invasive method to selectively identify and locate blood vessels within the PWS; (2) a means to deliver the heating laser energy to the appropriate spatial location for the required time; and (3) a strategy for heating blood vessels within the PWS volume imaged. We now discuss our current system approach to achieve these objectives.

2.4.1 Spectroscopic identification of blood vessels

Absorption reflectance spectroscopy with polarized light is the non-invasive method by which blood vessels are discriminated from other tissue in the PWS. The PWS (and skin in general) contains two dominant chromophores: melanin resident in the epidermis and oxyhemoglobin found in blood. Figure 2 shows that whole blood exhibits two strong absorption bands at 540 nm and 577 nm (with two other absorption peaks at 415 nm and 940 nm, not shown), predominately

due to the high concentration of oxyhemoglobin chromophore in the blood [Cheong, Prahl and Welch, 1990]. In comparison, the relative melanin absorption spectrum generally decreases with increasing wavelength (Figure 2) while its overall magnitude scales with epidermal melanin concentration. Dark and light skin have a melanin concentration of 0.023% and 0.008% by weight, respectively [Watts *et al.*, 1981]. Normalization of the blood absorption spectrum with respect to the melanin spectrum generates a high contrast ratio spectrum with a maximum and minimum relative absorbance at 577 nm and 640 nm, respectively. Thus a ratio of PWS images taken at these two wavelengths generates a high contrast image from which blood vessels are uniquely identified and their locations determined.

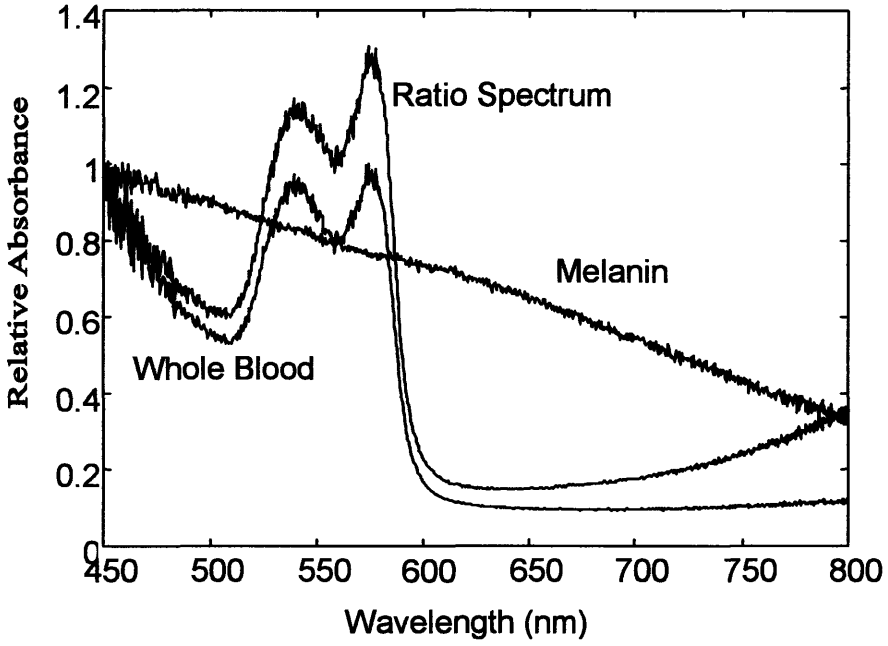

Figure 2: Relative absorbance spectra of human whole blood and melanin (black human hair) from 450 nm to 800 nm. The ratio of these two signals shows the enhanced contrast used to distinguish blood vessels from the surrounding tissue.

In addition to absorption, the scattering properties of skin must be considered in selection of an appropriate imaging scheme. The scattering coefficient of skin determines how much of the light delivered to the skin surface reaches the subsurface structures of interest (e.g. blood vessels). In general, longer wavelengths are scattered less and have greater penetration depths [Anderson and Parish, 1981]. Therefore, although the greatest hemoglobin absorption peak is at 415 nm, this wavelength is too short to penetrate to the depth of PWS blood vessels. At 415 nm,

the penetration depth, defined as the distance at which the energy incident on the skin is extinguished by 37% (1/e), is 100 μm. The penetration depth of 600 nm light is ~550 μm, which is close to the mean vessel depth of a typical PWS [Anderson and Parrish, 1981].

Image contrast is further enhanced when specular reflections from the skin surface are minimized. This is accomplished by illumination of the PWS with linearly polarized light and viewing the reflected light through a polarizer oriented orthogonal to the original polarization. Multiple scattering of the incident optical field by subsurface structures effectively depolarizes the backscattered light thus permitting discrimination between surface specular reflections from light reflected deeper in the tissue [Anderson, 1991].

2.4.2 Therapeutic laser

Effective heating of blood in a vessel requires absorption of optical energy by the blood in a vessel at a rate sufficient to overcome thermal losses and raise the local blood temperature to cause irreversible thermal damage. To achieve optimal opto-thermal coupling of radiation into a blood vessel, several criteria must be satisfied. First, the laser wavelength should coincide with one of the oxyhemoglobin absorption bands (415, 540, 577 or 940 nm) and, second, the laser light is focused to a diameter equal to the mean diameter of blood vessels in a typical PWS (ca. 50 μm). The $\times 10\,000$ smaller illuminated area compared with the conventional PWS treatment means the incident laser power can be substantially smaller to generate a similar photon flux incident on the targeted blood vessel so as to achieve a similar physiological outcome (vessel necrosis).

Chapter Three

Instrument Theory and Specifications

3.1 Optical reflectance spectroscopy

We have chosen optical reflectance spectroscopy (ORS) for the treatment of port wine stains because the absorbance for blood vessels is much higher than that of the surrounding tissue at the 577 nm wavelength. With ORS we may use a diffuse white light illumination of the PWS skin to detect the backscattered light at visible and near infrared wavelengths. We then filter this backscattered light to retrieve only the wavelengths of interest: one wavelength at a peak oxyhemoglobin absorbance, and a second outside the absorption band for normalization. Alternatively, we may use light-emitting diodes to illuminate the skin at specific wavelengths within (e.g. 565, 585 nm) and outside of (e.g. 635, 660 nm) the oxyhemoglobin absorption bands.

In either case, we direct each of the two wavelengths of interest to a photodetector, which converts the incident photons to electrons, generating a voltage or current signal during the integration time of the detector. Using analog or digital electronics, the ratio of the two signals is calculated. From this ratio signal, a threshold is used to generate a binary image of the region. This imaging coordinate space is then converted to the laser-scanning space to effectively deliver the heating laser beam energy to the appropriate vessel targets.

In imaging system design, the choice of optical components determines resolution and brightness of the image acquired by the photodetectors. The numerical aperture of the lens system affects both resolution and brightness. Numerical aperture (NA) is defined as:

$$NA = n \sin\theta \quad , \qquad (1)$$

where n is the refractive index of the material through which the light is propagating and θ is the collection angle of the lens. The expression $\sin\theta$ is the ratio of the lens radius to the lens focal length. NA impacts the spatial resolution according to the Rayleigh criterion, which states that

two points are resolvable when the maximum of one diffraction pattern overlaps the minimum of the other. The Rayleigh criterion results in a minimum lateral separation Δx, [Inoue, 1995]

$$\Delta x = \frac{0.61\lambda}{NA} \quad , \tag{2}$$

where λ is the optical wavelength. A similar analysis for two axially separate points of light results in a diffraction-limited axial resolution Δz,

$$\Delta z = \frac{2n\lambda}{(NA)^2} \quad , \tag{3}$$

In both cases, higher NA lens systems result in smaller resolvable features, meaning improved axial and lateral resolution. NA also impacts image brightness. In an imaging system, light is most efficient when the etendue E, is constant throughout the system. Etendue is the product of the area of the lens or other aperture and Ω, the solid angle, which is the cone of light collected by the lens. Solid angle is related to θ through the equation,

$$\Omega = 2\pi(1-\cos\theta) \quad , \tag{4}$$

Using Equation (1), the solid angle is related to NA in the following way,

$$\Omega = 2\pi(1-\sqrt{1-(\frac{NA}{n})^2}) \approx 2\pi(\frac{NA}{n})^2 \quad , \tag{5}$$

Since Ω scales with the square of NA, for a given lens area, E also increases with NA. Therefore, both resolution and brightness improve with high NA lenses. However, large NA optics can also cause significant chromatic aberrations. Aspheric lenses and composite lenses designed to reduce these aberrations are relatively expensive compared to standard spherical lenses.

3.2 Preliminary results: Identification of blood vessels

The optical system used for the preliminary results is a simple imaging system (Figure 3). The output of a 100 W tungsten white light source is polarized and then focused on the skin surface.

The reflected light is collected by an infinity-corrected (0.4 NA, 10x-magnification) objective that collimates the light reflected from the skin surface. The light then passes through a polarizer, which passes light of orthogonal polarization to the illumination. This polarization scheme blocks the specular reflection from the skin surface, making the underlying blood vessels of the camera image more apparent. The collimated light then passes through a liquid crystal tunable filter (Cambridge Research & Instrumentation, Inc. (Cambridge, MA), Varispec tunable filter, Model VS-05/30-HC-20-S). This filter can be programmed to wavelengths over a range of 450 to 720 nm. The 50% bandwidth for the two wavelengths used are 550 to 590 nm for the hemoglobin signal and 625 to 680 nm for the normalization wavelengths. The light exiting the tunable filter is then focused onto a charge-coupled device (CCD) array (Pulnix, (www.pulnix.com), TM-9701 progressive scan camera (768 × 484 pixels)) by an achromat to minimize chromatic aberration.

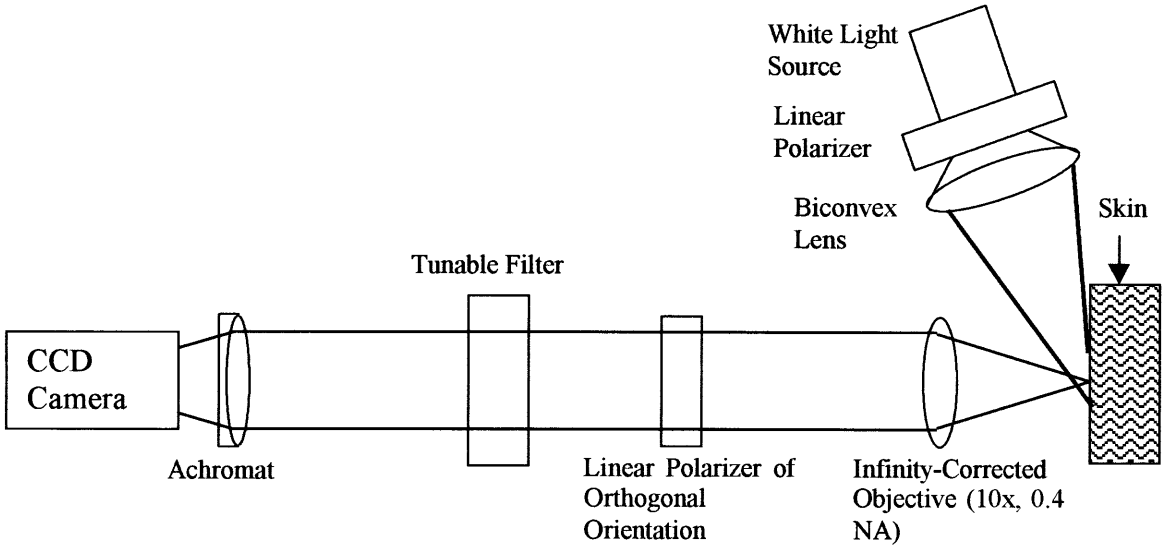

Figure 3: Schematic representation of optical system used to image and deliver laser energy to the blood vessels.

Figure 4 shows the contrast enhancement possible with this two-wavelength imaging scheme. Figure 4a is the reflected light absorption image of blood vessels in a mouse ear taken at the ~577 nm blood absorption band. Figure 4b is an image of the same region acquired with non-absorbing 650 nm reflected light and Figure 4c is the ratio image. Note the high degree of background suppression in the ratio image resulting in an enhanced blood vessel image contrast.

If the signal to noise ratio (SNR) is defined as the ratio of the blood vessel signal to the standard deviation of the background fluctuations, the SNR increases by approximately an order of magnitude (SNR 1.2 to 8.4) from an ORS (a) to an ORS ratio image (c).

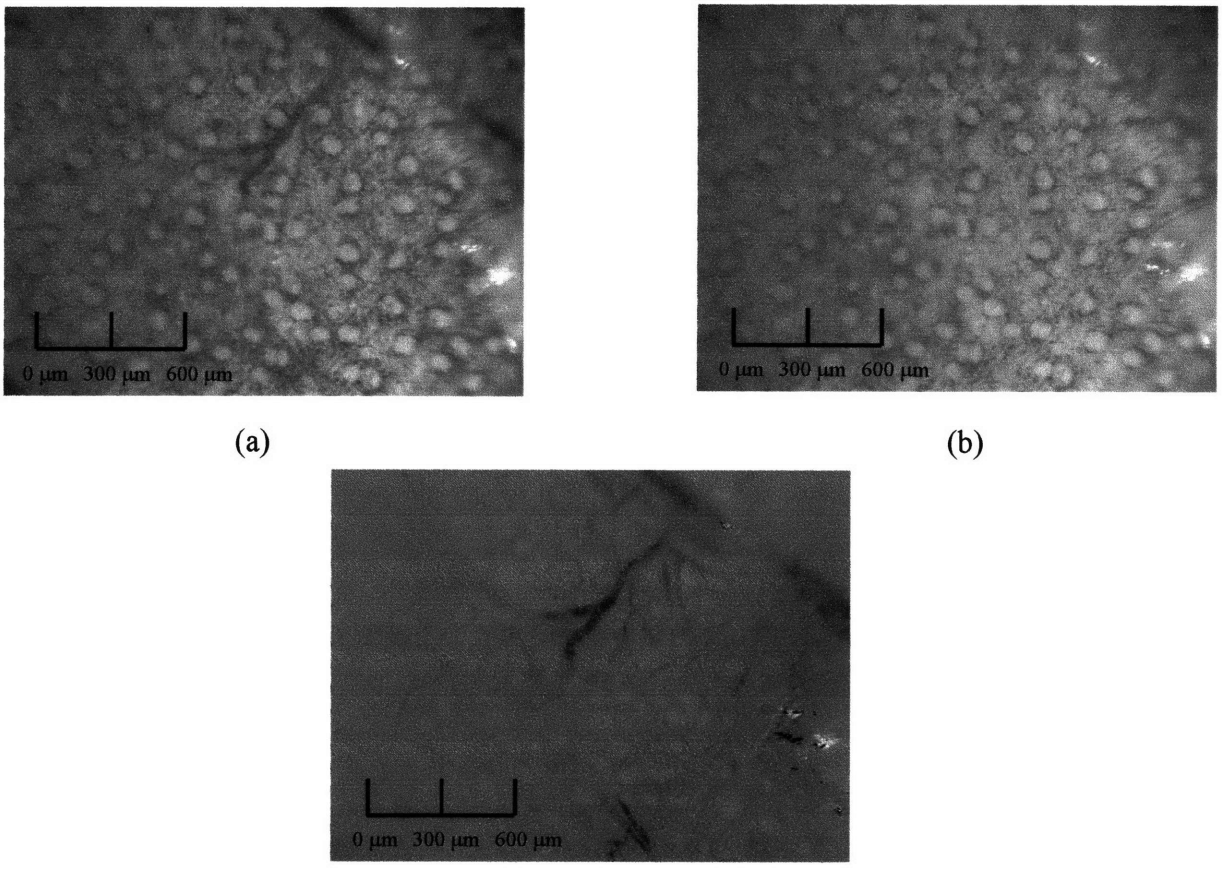

(a) (b)

(c)

Figure 4: Optical reflectance imaging of mouse ear blood vessels at (a) 577 nm and (b) 650 nm. Blood vessels appear in the upper right corner of the picture. The circular objects in the background are assumed to be hair follicles. (c) Dynamic range expanded ratio ORS image. Ratio taken of images acquired at 577 nm and 650 nm. Note high degree of background suppression and increased blood vessel contrast.

3.3 Laser-tissue interactions

The three primary considerations for laser-tissue interactions for this application are thermal relaxation time, energy necessary to coagulate the blood, and the absorption and scattering of light by various skin structures.

3.3.1 Thermal relaxation time

Energy absorbed by the vessels is converted primarily to thermal energy if the ratio of illumination time, τ_{ill}, to the tissue thermal relaxation time, τ_r is greater than one. The illuminated region is in thermal equilibrium with the surrounding tissue and a significant amount of heat diffuses out of the blood vessel. Therefore, it is desirable to deliver the laser energy to the blood vessels in a time shorter than the thermal relaxation period. However, if $\tau_{ill} << \tau_r$, energy conversion is primarily adiabatic and substantial mechanical damage to the vessel can result.

The thermal relaxation time for a blood vessel of diameter, d, is

$$\tau_r = \frac{d^2}{16\alpha} \quad , \tag{6}$$

in which the thermal diffusivity, α, is

$$\alpha = \frac{\beta}{\rho c} \quad , \tag{7}$$

and β, ρ, and c, are the thermal conductivity [W/m/K], density [kg/m^3], and specific heat [J/kg/K], respectively. For tissue composed of 70% water, the value of thermal diffusivity, α, is 1.15×10^{-7} m^2/s [McKenzie, 1990]. Therefore, assuming a 50 μm diameter blood vessel (typical of many PWS), the thermal relaxation time is ~1 ms.

3.3.2 Laser coagulation of blood

An estimate of the laser power required to coagulate the blood in a typical PWS blood vessel with a focused laser beam can also be calculated. Assuming (1) thermal equilibrium between the blood vessels and surrounding tissue, (2) a laser illumination diameter equal to the blood vessel diameter (50 μm), and (3) a blood specific heat and density close to that of water, the energy needed to heat a volume of blood enclosed in the illuminated volume to its coagulation temperature is given by:

$$E = mc\Delta T \quad , \tag{8}$$

where m is the mass of the region of blood treated, c is the specific heat (assumed to be close to water, ~4.2 kJ/(kg K)), and ΔT is the temperature rise required for coagulation of blood, ~40 K above ambient body temperature.

The mass, m, of blood heated is given by:

$$m = \rho V \quad , \tag{9}$$

$$V = \pi(r^2 d) \quad , \tag{10}$$

where ρ is the density of blood, again assumed to be similar to water (~1000 kg/m^3). The volume V is given by the area of the beam illuminating the vessel (πr^2, where the radius r of the laser spot is 25 μm), and d is the blood vessel diameter, assumed to be 50 μm for these calculations. These equations demonstrate that ~16 μJ is the necessary energy incident on the blood vessel to cause coagulation. With a ~1 ms laser dwell time (on the order of the thermal relaxation time), this corresponds to an absorbed power of ~16 mW.

These calculations do not consider heat losses as blood flowing through the vessels carries the thermal energy away from the treatment area. For vessel diameters of ~1 mm, estimated blood flow rates are ~10^{-6} m^3/s [Whelan *et al.*, 1995]. Theoretical modeling and actual measurements in tissue phantoms mimicking the heat transfer across the vessel wall to the flowing blood, showed a temperature increase in blood temperature from 37 °C to ~40 °C, when the outside wall was heated to with a 2W Nd:YAG laser over a time scale of 800 s. However, in the millisecond time scale over which laser energy will be delivered in the Smart Scalpel system, the heat transfer to the flowing blood is negligible. Therefore, we can neglect heat losses due to blood flow.

3.3.3 Laser attenuation due to absorption and scattering

Since these blood vessels are located in the dermis, ~500 μm below the skin surface, the light incident on the skin surface will be attenuated, through absorption and scattering as it propagates through the epidermis to the dermis, where the blood vessels are located. Applying a simple

Beer's law absorption/scattering model, the estimated laser power incident on the skin required to generate the specified temperature rise is given by:

$$P = P_o e^{-(\alpha_s + \alpha_a)h} \quad , \qquad (11)$$

where P is the power required to coagulate the blood (16 mW), P_o is the power incident on the skin, α_s is the human dermis scattering coefficient (225 cm^{-1} at 633 nm) [Cheong, 1990], and α_a is the blood absorption coefficient (~13 cm^{-1} at 580 nm), and h is the depth of the blood vessels from the skin surface (~500 μm). The parameters α_s and α_a have the dimension of [1/L], and the mean free path is the value of h equal to $1/(\alpha_s+\alpha_a)$. Over the distance of one mean free path, the ratio of P to P_0 is e^{-1}, so that P is approximately 35% of P_0. Beer's law offers the result that ~2 kW of power must be incident on the skin within a 50 μm diameter spot (2×10^{-9} m^2) to sufficiently heat the blood vessels and cause coagulation. Since most beams have a ~1 mm diameter, a laser power of ~1 watt will be required to heat the blood vessels. Several types of lasers exist with this optical power and a wavelength coincident with the oxyhemoglobin absorption band suitable for inclusion as the Smart Scalpel therapeutic laser.

3.4 Control strategy

We have considered several Smart Scalpel imaging and laser targeting strategies, which can be classified into three basic methods. The first is point spectroscopic detection combined with serial scanning to cover affected area. The second is full-field imaging with servo-controlled beam steering. The third strategy, which has been selected for this application, involves line imaging and point laser scanning. The trade-offs among these three strategies will be further developed in the following sections, and our reasons for selecting the line scan strategy will be discussed.

Effective implementation of any of these laser targeting strategies demands minimal relative motion between the image area and the PWS during the image acquisition, processing and targeting sequence. Tremor is the major source of motion for which the Smart Scalpel must compensate. The result of varied causes, tremor can have a maximal frequency component of 10 Hz with a quasi-sinusoidal displacement that varies across body parts (hands, feet, etc.) and

between different people [Elble and Koller, 1979]. Accordingly, the maximum number of targets, n, addressed in one scan is expressed as,

$$n = \frac{T_{move}}{(T_{exposure} + T_{acquisition} + T_{computer} + T_{galvos} + T_{ill})} \quad , \tag{12}$$

where T_{move} is time period of skin displacement (100 ms for a maximum 10 Hz tremor frequency) Time delays in the feedback loop include: $T_{exposure}$, the integration time of the line array; $T_{acquisition}$, the time required to acquire and convert the photocurrents to an output voltage; $T_{computer}$, the data acquisition and processing time of the computer; T_{galvos}, the step response of the two-axis scanning system; and T_{ill}, the time required for the laser to thermally treat the blood vessels. For the ideal system, the longest time delay should be the laser illumination time (~1 ms), which sets an upper limit of ~100 targets that can be treated within the tremor period.

3.4.1 Serial point-scanning approach

This serial approach relies sequentially scanning a point illumination, using a point detector to determine whether spatial location contains a PWS blood vessel, and if a blood vessel is present, scanning the laser beam to that location for treatment. Figure 5 illustrates one implementation of this approach.

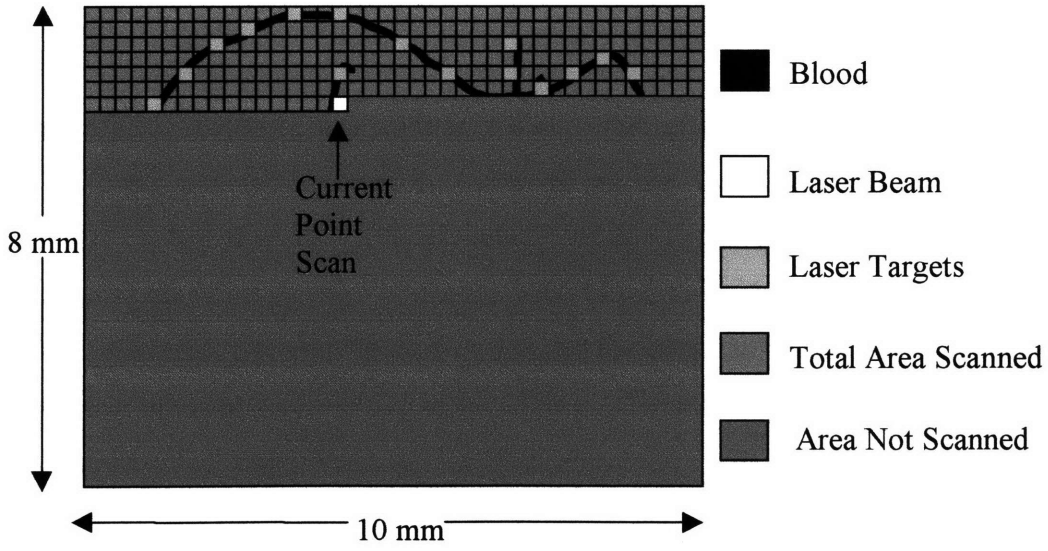

Figure 5: Illustration of point imaging and point laser-scanning approach.

This approach has the advantages of simplicity and speed. The imaging illumination and treatment laser can both be positioned with the same scanner. Also, because only one pixel is read before each laser treatment, there is little delay between image acquisition and treatment. Therefore, any relative motion causes minimal shift between the time the image is acquired and the laser energy delivered. We anticipate that an instrument employing this strategy could be easily miniaturized. The physician could scan the Smart Scalpel over the tissue surface, treating 50 μm regions with each laser pulse. Alternatively, the instrument could be stationary and employ a two axis scanning system to treat a $\sim 10^{-4}$ m^2 region as the surgeon holds the Smart Scalpel on the skin surface. Once the first region is treated, the physician could move the instrument to a new area and repeat the treatment process for the entire PWS lesion.

The disadvantage of this strategy is that no spatial information can be acquired in advance of the laser delivery, so that pattern recognition of individual blood vessel is not possible. In treatment of telangiectasias (skin of larger, more sparsely populated blood vessels than PWS), physicians trace individual blood vessels from the smallest branches inward to the large supply vessels. This strategy routes the blood flow away from the branches, allowing more effective heating of the vessels with the laser light [Tope, personal communication, 1999]. It is unknown whether such a strategy will be required for PWS treatment, but a system with the flexibility for both feed forward and feedback schemes played an integral role in selection of a scanning scheme.

3.4.2 Full-field approach

The second approach considered is a stationary device that images a two-dimensional field, on the order of 10^{-4} m^2, and targets specific locations on the vessel network. Figure 6 is an illustration of this control strategy. The advantages of this approach are simplicity in imaging strategy and acquisition of information about the PWS blood vessel in advance of laser targeting. This facilitates pattern recognition of blood vessels, so the laser can be scanned along individual blood vessels rather than randomly hitting points along different blood vessels.

One disadvantage of this full-field approach is the speed sacrificed in image acquisition. This time delay may cause increased errors, since there is more time for relative motion between the patient and the instrument. For this approach, we considered a 2-dimensional CCD array as our

detector. Current camera technology exists to achieve high resolution over a large field of view (~1 Mpixel) but cameras with high enough frame rates (~30 frames/s) to avoid serious problems with relative motion between the instrument and patient are very expensive. Computer hardware is capable of handling high data rates (PCI bus bandwidth = 132 Mbytes/s burst, ~50 Mbytes/s sustained), so as technology improves and camera prices decrease in the future, this full-field approach may become feasible.

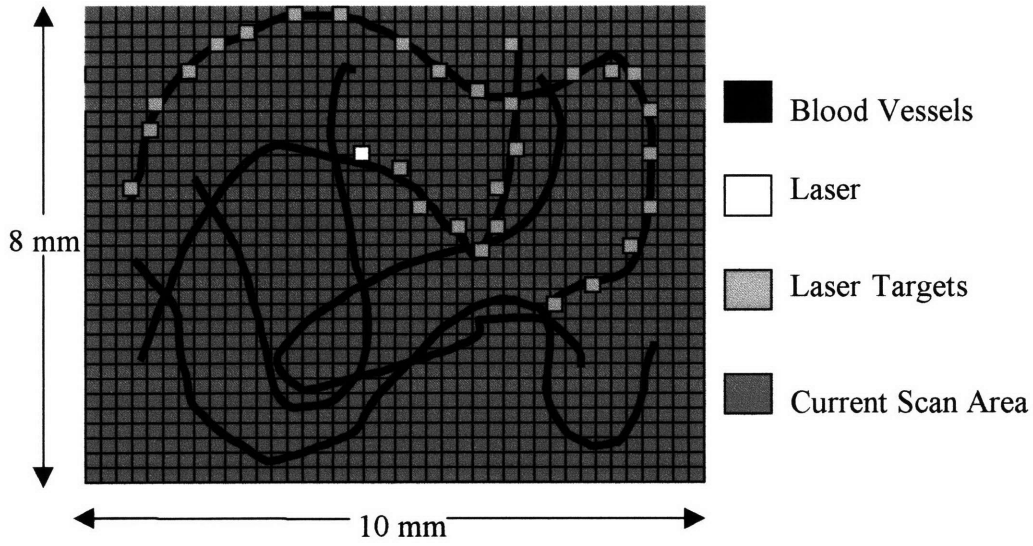

Figure 6: Illustration of full-field imaging and point laser scanning strategy.

3.4.3 Scanning of line illumination

The final approach considered, and the one that is implemented in the Smart Scalpel prototype aims to combine the positive attributes of the serial and full-field imaging approaches. The line imaging approach (Figure 7) allows dynamic control of the size of the imaged area. If the PWS region contains very few blood vessels, the number of targets per unit area is lower. Because the number of targets that can be treated in one imaging and treatment iteration is contrast, this means a larger area can be treated within the time in which relative movement is negligible. Alternatively, if the PWS region contains a dense network of blood vessels, the number of lines scanned per iteration could be reduces to effectively treat the great number of targets in that region.

This flexibility is helpful in optimizing the trade-off between treating the largest area for each scan versus minimizing the time delay between when the image is acquired and the time the laser

energy is delivered to the identified targets. The frequency and magnitude of relative motion between the instrument and patient is largely unknown and variable. This variability arises from many sources, including location of the PWS (since different body parts move differently), position of the patient, calmness of the patient, etc. Also, the density of blood vessels within the PWS is highly variable. In addition, the line imaging and point laser scanning technique also provides information about the targets in advance of the laser scanning. This may be important if some degree of blood vessel pattern recognition is required in advance of laser scanning.

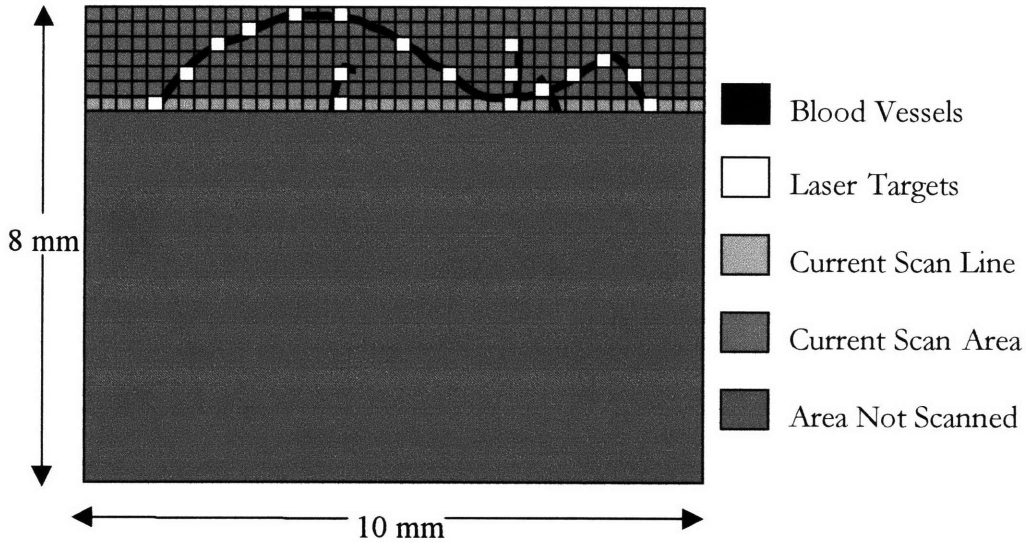

Figure 7: Illustration of line imaging and point laser-scanning strategy.

Chapter Four

Smart Scalpel Preliminary Design

4.1 Line illumination

A diagram of the optical layout for the prototype Smart Scalpel is shown in Figure 8. The desired resolution for the imaging system is 50 μm, the average PWS blood vessel diameter. A treatment area of ~10^{-4} mm^2 has been specified to conveniently interface with the physician and patient. This is the same size as the laser beam diameter used in current PWS removal.

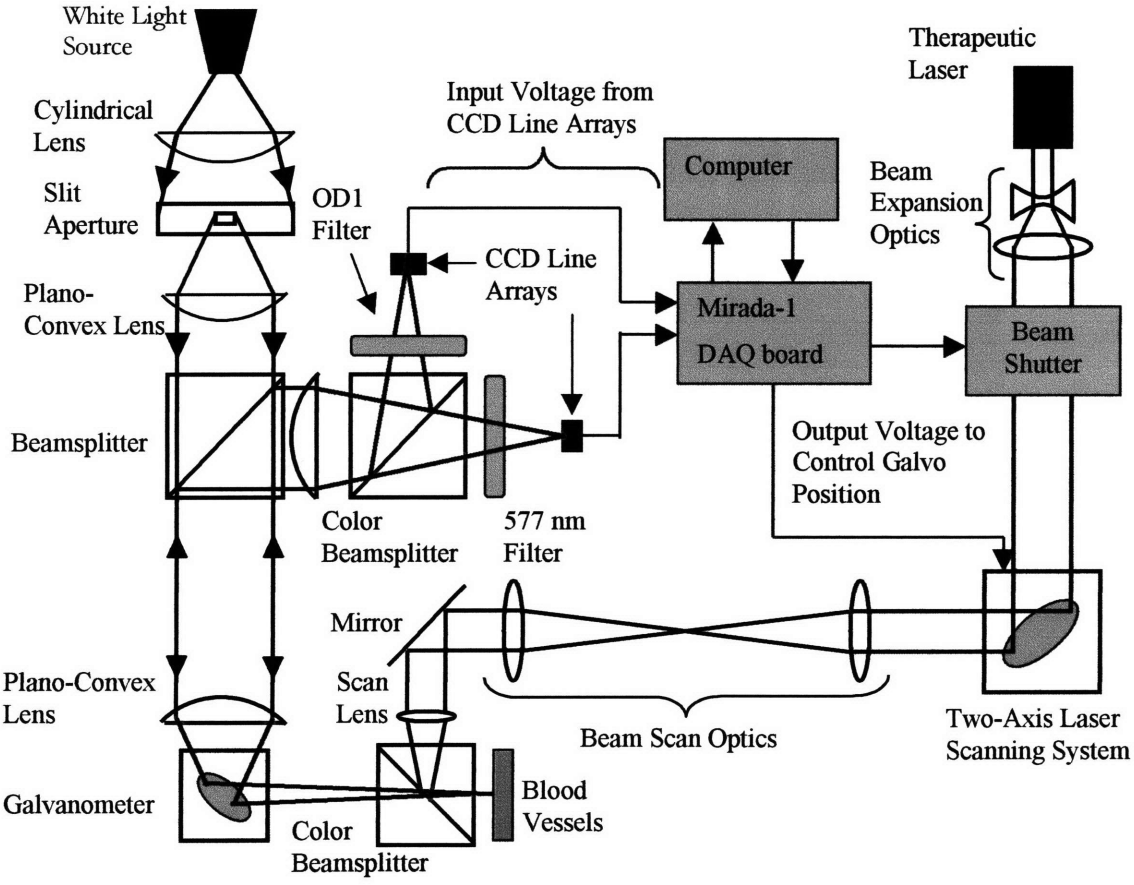

Figure 8: Schematic representation of preliminary design for Smart Scalpel beam scanning and imaging systems.

Light from a fiber optic-coupled 100 W xenon light source illuminates an optical system configured to generate a line of polarized white light on the skin. The output of the fiber bundle is focused onto a slit aperture (50 μm by 6 mm). The line illumination passes through a plano-convex lens to collimate the light. This collimated light is directed toward a polarizing beamsplitter and the line is focused with a planoconvex lens onto the skin. A galvanometer-mounted mirror scans the illumination line across the skin surface and also de-scans the reflected light to the stationary photodetectors. To physically get the sample to the focused line of light, a relatively long focal length lens was required for the final focusing of the illumination. This meant the line image had to be magnified by a factor of two, which sacrificed the resolution that could be achieved between lines.

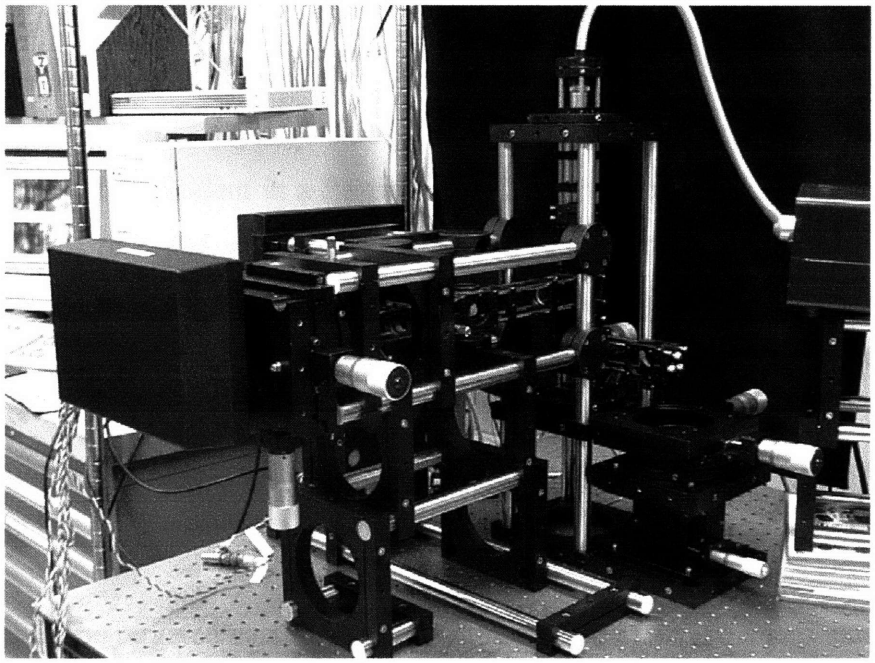

Figure 9: Photograph of Smart Scalpel prototype system.

4.2 Imaging detectors

The light reflected and backscattered from the skin at each galvanometer scan position is de-scanned by the galvanometer, reflected by the polarizing beamsplitter and imaged by a planoconvex lens through a color beamsplitter onto two linear CCD photosensor arrays. Wavelengths shorter than 630 nm are directed toward one array and further spectrally filtered with a 577.8 nm bandpass filter (50% bandwidth 8.8 nm) to generate the blood (oxyhemoglobin)

signal. Wavelengths longer than 630 nm filtered with a neutral density filter (optical density 1) to match the intensity of light delivered to the green channel sensor. This attenuated red light is transmitted to the second array to generate a normalization signal against which the oxyhemoglobin signal is compared. The CCD sensors used for this system are 1024 element CCD spectroscopy line sensors (EG&G Reticon S Series, (www.egginc.com), 25 μm × 2.5 mm pixels, ~16 bit dynamic range). Since the desired resolution for the imaging system is 10 μm, the overall magnification of the imaging system is 2.5, so that one pixel on the array corresponds to 10 μm on the skin surface. This resolution is sufficient to image the 50 to 100 μm blood vessels, which will be the smallest targets in the PWS treatment.

4.3 Data acquisition and control: hardware and software

The photosensor outputs are recorded by the analog-to-digital converters (100 kS/s @ 18 bit/sample) of a home-built data acquisition board (Mirada-1, developed by Dr. Martel in our laboratory) on a PCI bus resident in a Pentium II PC and controlled by a program written in C. After a line image is recorded, a command is sent via the Mirada board 18 bit digital-to-analog (D/A) converters to rotate the scanning galvanometer to a new position and a new line image is recorded. After the optimal number of line images is acquired, a ratio image is computed and a threshold is set to determine the blood vessel locations. The optimal number of lines is determined by the density of targets in the imaging field, since the total number of targets that can be treated in a given time is constant.

The coordinates of the targeted vessels are sent via the Mirada D/As to a two-axis laser scanning galvanometer to direct the heating laser beam onto blood vessels selected in the field of view. The two-axis galvanometer system was chosen, instead of faster resonant scanners, to provide random access positioning to all points in the field of view. In addition, one D/A channel is used to control an electro-optic beam modulator (Conoptics 380 Series; www.conoptics.com, ammonium dihydrogen phosphate liquid crystal electro-optic light modulator). Because the line illumination is not entirely constant across the width of the scan, the two-wavelength normalization also improves image uniformity.

Processing of the ratio image to identify blood vessels is, at present, algorithmically straightforward. A histogram analysis of the ratio image sets a binary threshold in which all pixels below the threshold value (corresponding to high absorption) are identified as blood vessels. The vessel position in the image field of view is calculated and converted to target coordinates for the two-axis laser scanning system. The step response time of the current laser-scanning system is ~1 ms and is comparable to the estimated blood vessel thermal relaxation time, τ_r. Therefore, during the transit time between targets, the electro-optic beam modulator blocks the laser beam to prevent heating of the tissue between blood vessels.

4.4 Laser beam scanning

The heating laser delivery subsystem of the Smart Scalpel is flexible in that any laser can be used with the system. The laser source can be a continuous wave or millisecond-pulsed laser at a wavelength of substantial hemoglobin absorption and minimal scattering and absorption by other tissues. Laser sources considered to date include: argon (488 or 514.8 nm), frequency doubled Nd:YAG laser (532 nm), and a 985 nm laser diode, or a millisecond pulsed dye laser tuned to 577 nm or 585 nm. The laser beam is first expanded to the maximum beam diameter that can be scanned by the mirrors on the two-axis galvanometer system. Standard beam scanning optics are used to transmit the telecentric location between the two galvanometers to the final scan lens, which converts the beam rotation to a displacement scanned on the surface of the skin. The final laser spot is to be approximately 10 to 50 μm to provide the desired spatial resolution for blood vessels targets ranging from 50 μm to 1 mm.

In a clinical setting, a fiber bundle may be used to transmit this line illumination and laser energy from the Smart Scalpel system to the skin surface, so the instrument is remote from the physician and patient. Because of the line illumination, control strategies employing pattern recognition and feed-forward control strategies would require a coherent fiber bundle to guarantee the line scanned on one end of the bundle corresponds to a line scan on the skin surface. If such strategies are not employed and blood vessels can be targeted randomly, a coherent bundle is not required.

Chapter Five

Imaging System Results

5.1 Preliminary results

5.1.1 Resolution and contrast

To quantify the resolution of the system, a standard test pattern of horizontal and vertical bars of known dimensions was scanned. The imaged reticle (Spindler & Hoyer; Milford, MA) is shown in Figure 10. The region in the box is what is typically scanned in the images appearing in future sections(~ 8 mm × 10 mm).

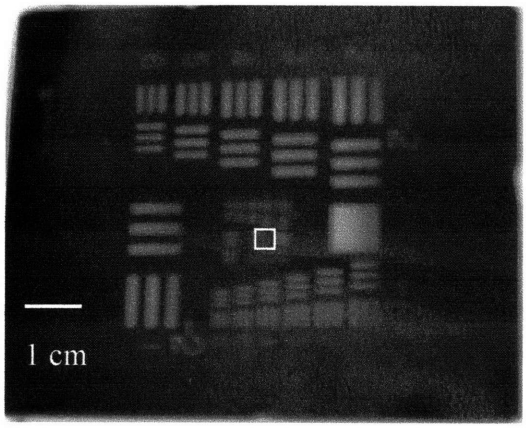

Figure 10: Image of reticle used to quantify vertical and horizontal resolution of the Smart Scalpel imaging system. Region in the center box represents the area imaged for scans in the following section.

The line scan image (2 kHz pixel rate, 0.5 s integration time) of a standard bar target was used to quantify the lateral resolution of the imaging system. Figure 11 displays the image generated from the green sensor. Non-uniformity in the line illumination was compensated for by normalization against the image of a uniformly reflecting target (mirror). Plots of pixel values along lines parallel and perpendicular to the line illumination (lines A and B, respectively) show the difference in lateral resolution between the two orthogonal directions. The horizontal lines (plot B) are parallel to the scanned line of light, while the vertical lines (plot A) are perpendicular to this line scan. Because the line scanned on the surface of the reticle is approximately 100 μm

(50 μm slit with 2× magnification), the resolution of horizontal lines is fundamentally limited by the slit diameter. This fundamental limitation in horizontal resolution was verified by decreasing the distance between consecutively illuminated lines on the sample. Decreasing the step size between lines from 28 μm to 14 μm had no effect on either vertical or horizontal resolution of these images. The vertical line resolution is determined by the magnification of the imaging system and the pixel dimensions of the CCD line array.

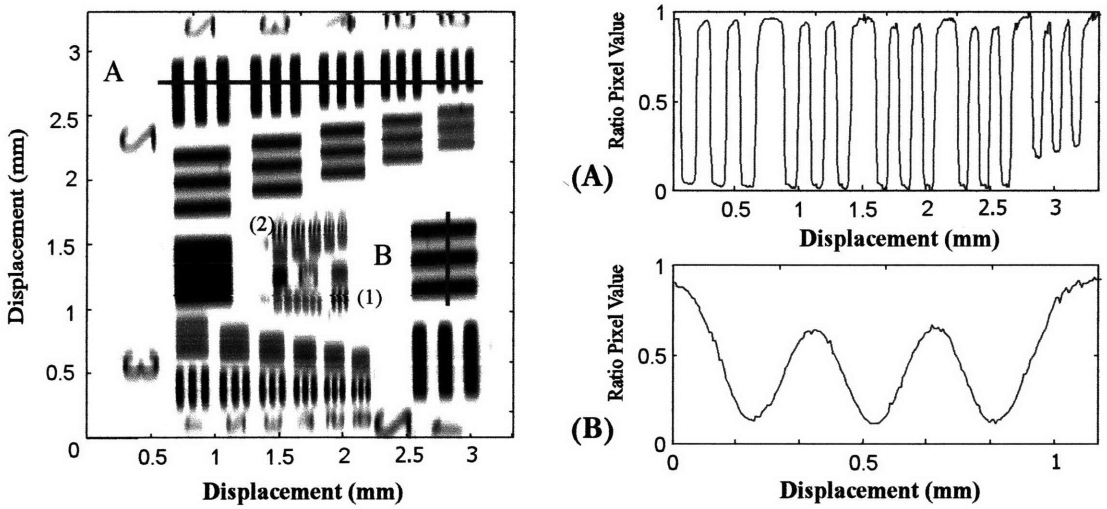

Figure 11: Test pattern to quantify resolution and sensitivity of imaging system. (A) Vertical lines (perpendicular to line scan). (B) Horizontal lines (parallel to line scan).

We use the modulation transfer function (MTF) to quantify the resolution of our system. The MTF is the ratio of the modulation amplitude at the output to the modulation at the input of the optical system and is independent of the DC offset of the modulation [Goodman, 1982]. To calculate the MTF over a range of spatial frequencies, where spatial frequency is defined as the number of spatial modulations per unit length. To generate the MTF, the maximum and minimum reflection signals were measured, and the difference between the two values was calculated and divided by two. The modulation of the spatial frequency with the greatest amplitude was used as the input signal and therefore the denominator the MTF. For each spatial frequency, the numerator was the amplitude of the modulation for that specific frequency.

The MTF versus spatial frequency of the imaging system illustrates the substantial difference in resolution between the two orthogonal directions (Figure 12). The vertical resolution is currently

limited by the slit width (100 μm). Decreasing the width of the line illumination should increase the vertical imaging resolution but may correspondingly decrease image brightness, as less light is illuminating the sample, and therefore the CCD array. Because the image resolution parallel to the line illumination fell short of the system specification of identification of 50 μm features (average PWS blood vessel diameter), we decided to complete a further iteration of optical design to improve the system resolution.

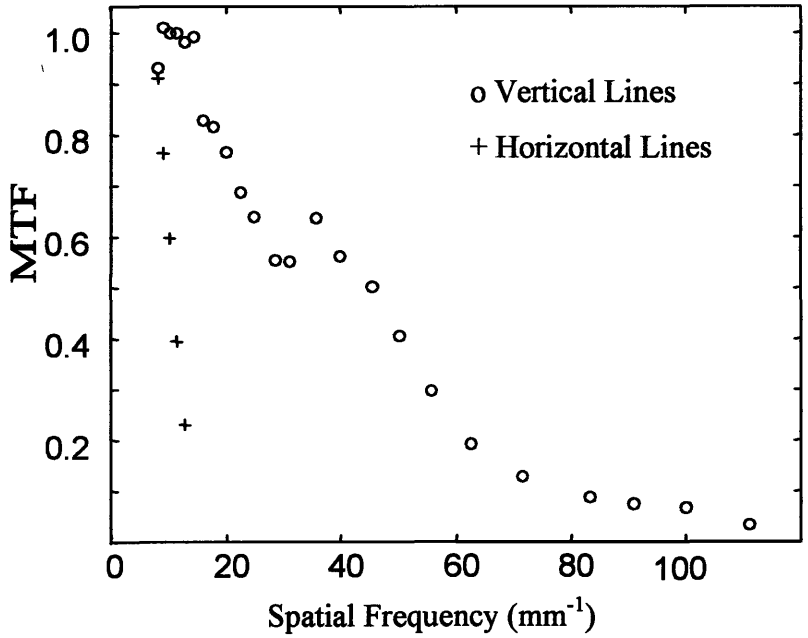

Figure 12: Preliminary image contrast results over a range of spatial frequencies.

While the contrast generally decreases with increasing spatial frequency, an unexpected increase in image contrast is observed between 30 and 40 lines/mm. The MTF was generated from bar patterns located in different parts of the line scan image shown in Figure 10. The 30 and 40 lines/mm bars are labeled as numbers (1) and (2), respectively Figure 10.

5.1.2 Blood vessel imaging

Using the first Smart Scalpel prototype, preliminary blood vessel images from the ear of a live mouse were generated (Figure 13). To generate this image, a 500 μm slit was used to allow greater illumination intensity, and the integration time was doubled from 0.5 s to 1 s. These modifications were required because of the decreased reflectance signal from tissue versus the mirror surface of the reticle, which was imaged with a 50 μm slit. This means image resolution

was sacrificed to a great extent. Also, the contrast between the blood vessel and background signals was only ~6%, with contrast defined as (max-min)/(max+min). The image shown has been dynamic range expanded to show blood vessel features. Given this small contrast, the threshold operation would be very difficult to generate the binary image of blood vessels and background.

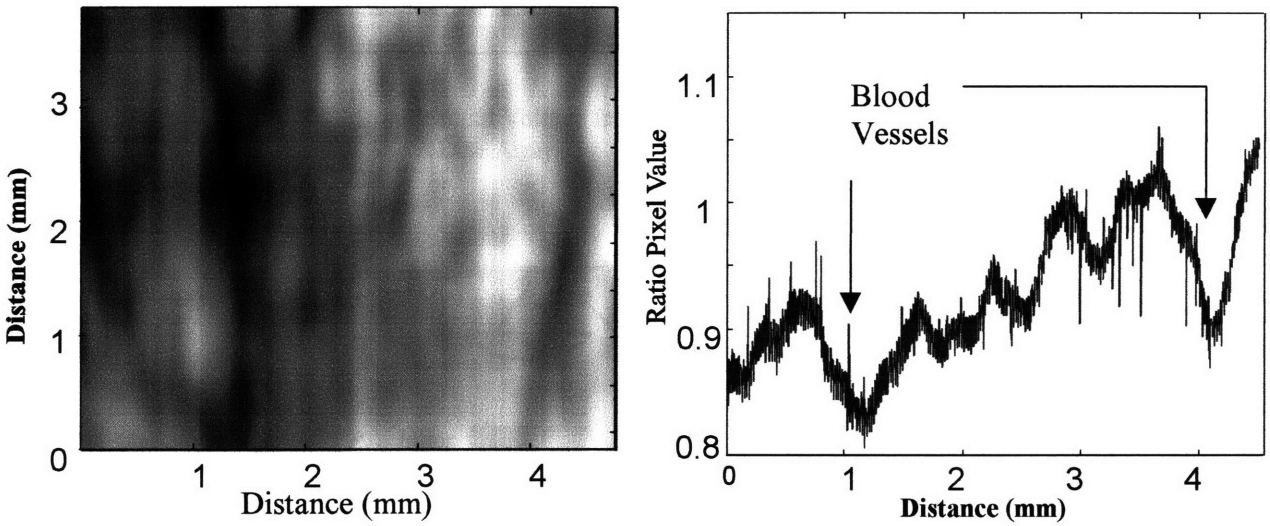

Figure 13: Preliminary blood vessel image and line plot of ratio values for line scan at the 2 mm vertical position of a live mouse ear.

5.2 System improvements and new results

Because these preliminary results were judged to be unsatisfactory in terms of resolution and contrast, several improvements were made. First, a 300 W xenon light source replaced the 100 W light source used in the previous version. The output of the xenon source was transmitted to the Smart Scalpel system through a circular to rectangular cross-section fiber bundle. This rectangular cross section (0.8 mm by 9.7 mm) couples more efficiently with the rectangular slit through which the light is focused and onto the material to be imaged.

The optical system was also redesigned (Figure 14) to more efficiently couple light transmitted from the slit aperture to the imaged material. Plano-concave lenses were added in two locations to maintain unity magnification of this transmission system and allow the imaged material to be far enough away so it would not spatially interfere with the mechanical structure of the optical system. Finally, the narrow band interference filters (peak wavelength 578.9 nm, 50%

bandwidth 8.8 nm) was replaced by broader bandpass filters for the green (peak wavelength 560 nm, 50% bandwidth 60 nm) and red (peak wavelength 650 nm, 50% bandwidth 50 nm) channels to transmit more light to the green and red sensors. The new green filter has a transmission band that overlaps both the 540 nm and 577 nm oxyhemoglobin absorption bands.

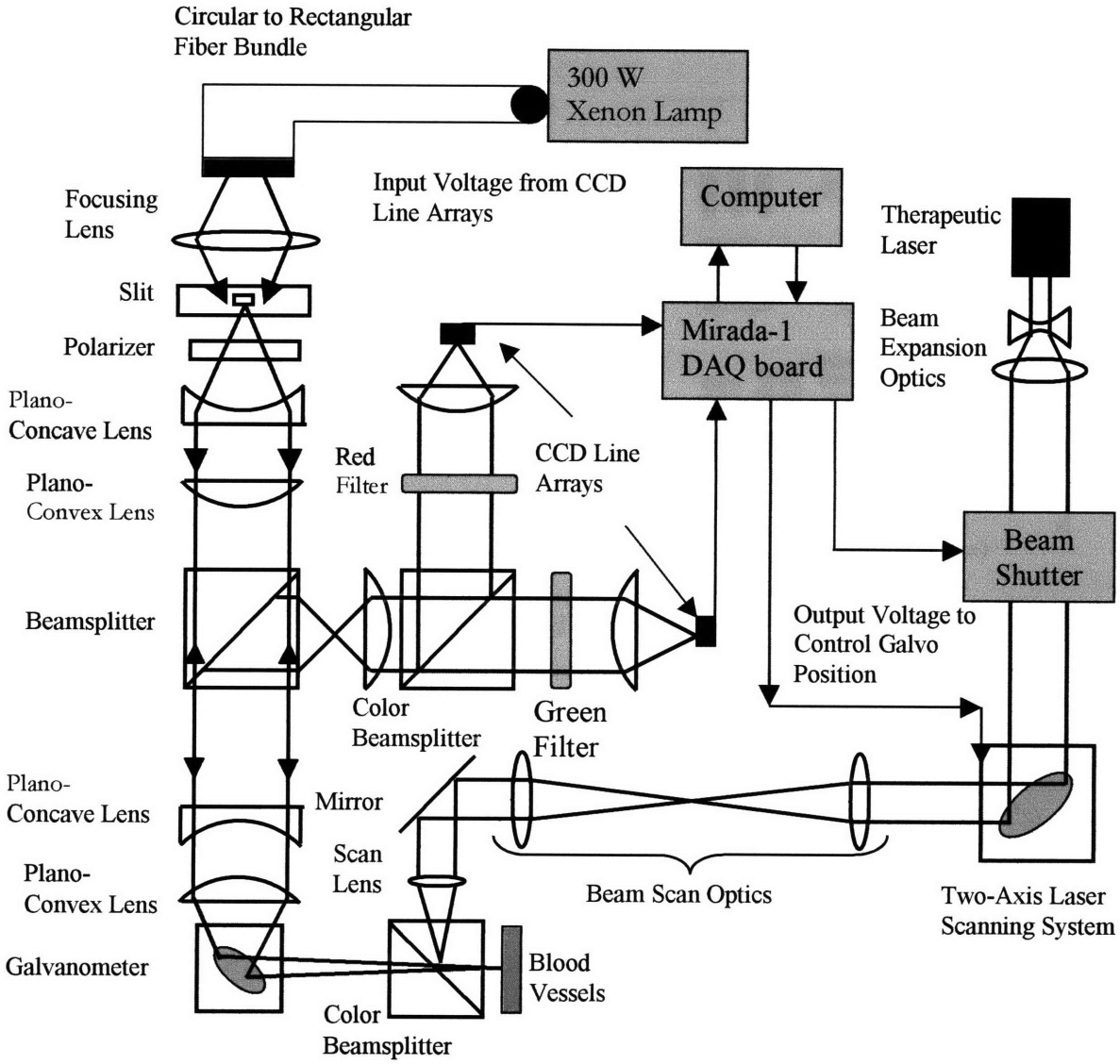

Figure 14: Schematic of Smart Scalpel prototype with design improvements.

In this imaging system, the etendue is limited by the aperture and long focal length of the final lens that focuses the light reflected from the tissue onto the CCD line arrays. This final focusing lens has a 0.083 NA (focal length, 150 mm; diameter, 25 mm), and this low NA lens fundamentally limits the resolution and brightness of the image. However, this lens was chosen

to achieve the magnification necessary to match the line illumination on the sample to the area of the CCD line array. The slit dimensions are 50 um by 6 mm, while the array is 2.5 mm by 25 mm. Therefore, the slit must be magnified ~5 times to fill the array. The ratio of the focal length of the final focusing lens to the initial collection lens (focal length, 30 mm) provides the magnification necessary to match the reflected light to the line array.

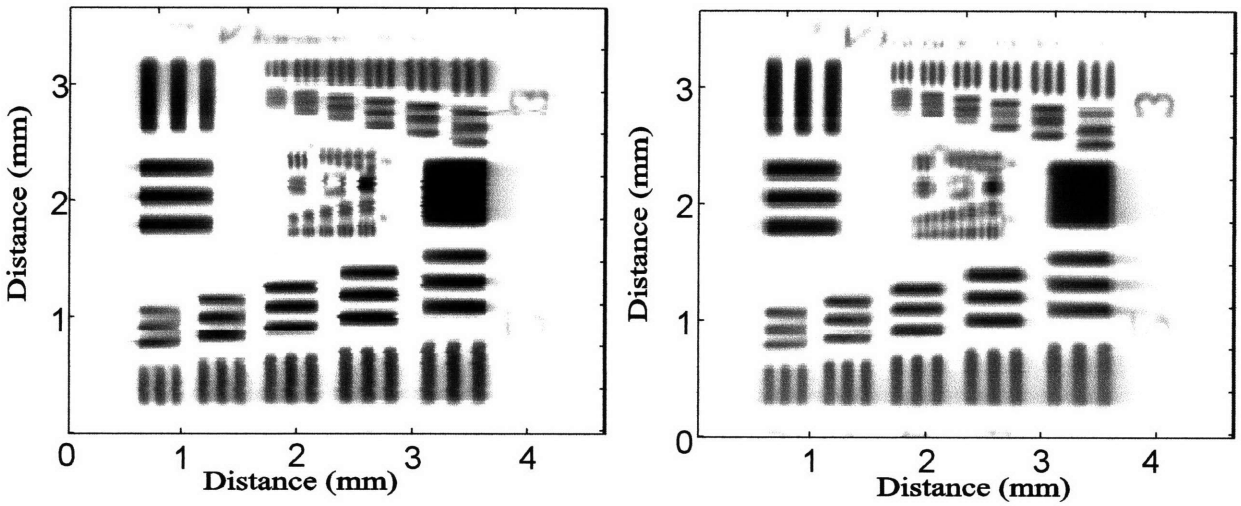

Figure 15: Test pattern to quantify resolution and sensitivity of imaging system for green channel (left) and red channel (right).

The new reticle images on the red and green channels are shown in Figure 15. The modifications made resulted in much improved resolution for horizontal lines compared with the original results. However, there was an apparent smearing of the image between the dark regions of the image. The cause of this is unknown, but is speculated to be a chromatic aberration or perhaps an unwanted back-reflection off one of the optical components. This impacts image fidelity and decreases the contrast between reflecting and transmitting regions of the reticle.

The MTFs for the horizontal and vertical lines of the green and red channels are plotted in Figure 16. The modifications made to the system resulted in much more comparable trends in the MTF for the horizontal and vertical directions. Another positive result is that both channels show similar trends in the horizontal and vertical directions.

However, this MTF shows greater non-uniformity than the previous imaging system. While the MTF for the horizontal lines generally decreases with increasing spatial frequency, there are unexpected increases in image contrast between 8 and 9 lines per mm and between 15 and 16 lines per mm for both channels. One hypothesis for this is that regions along the flat plane are slightly out of focus because the galvanometer scanning an arc across a flat plane. However, the data collected for the MTF versus depth (Figure 19) suggest that this is not the case. The distance from the scanning galvanometer mirror to the sample is ~120 mm, while the area scanned is ~10 mm. This means the difference in path length from the mirror to the sample is ~100 μm. Figure 19 demonstrates that this small displacement does not significantly affect the MTF.

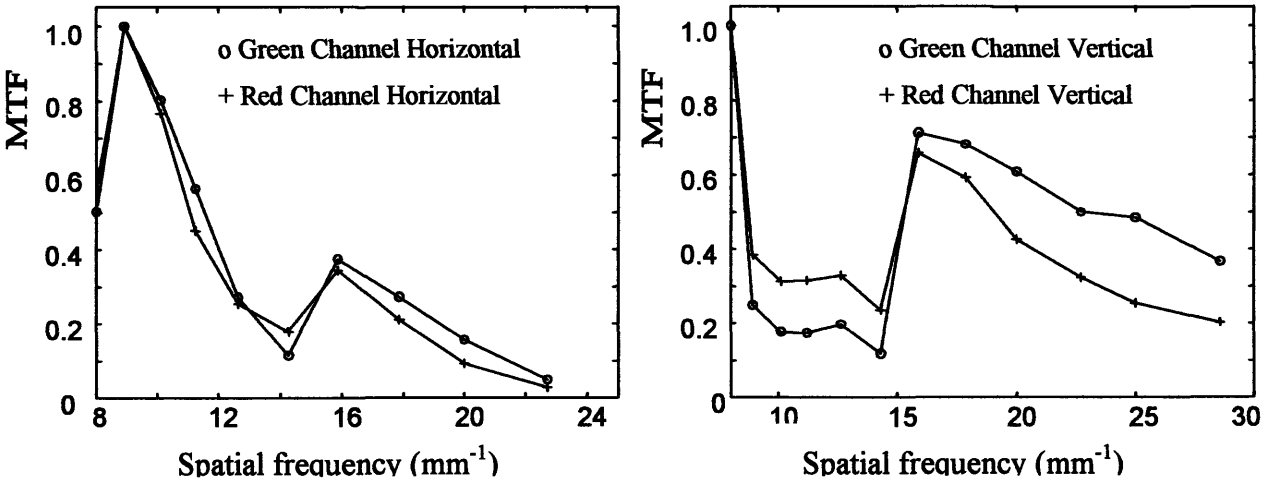

Figure 16: Modulation transfer function for horizontal (left) and vertical (right) lines on the red and green channels.

Another possible explanation for the lack of uniformity in the MTF is a variation in the smearing that occurs throughout the imaged area. The two MTFs show a uniformly decreasing trend along the targets located in the same regions, with discontinuities occuring from one region of lines to the next. Perhaps unwanted back reflections cause this smearing and are greater in some regions than others. Examination of Figure 15 reveals greater apparent smearing in the top line of vertical bars (spatial frequencies 16mm^{-1} through 24 mm^{-1}) than in the bottom line (spatial frequencies 8mm^{-1} through 14mm^{-1}), while the red channel shows the opposite trend. The reason

for this is unknown, but may provide a clue to understanding the nonuniformity in the MTF for these spatial frequencies.

5.3 Contrast vs. Spatial Location

Given the unexpected shape of the MTF, efforts we made to characterize variations in contrast across the along the lateral (perpendicular and parallel to the line scan) and in the axial direction. Results are shown and discussed in the following sections.

5.3.1 MTF versus lateral position

The MTF across the x (perpendicular to scan) and y (parallel to scan line) axes were plotted for the 125 um horizontal and vertical lines (Figure 17). Horizontal lines are parallel to the line scan and vertical lines are perpendicular. The x-direction plots were generated by moving the reticle across the imaging field, and the zero point is where the 125 um bars were located in the center of the imaging field. The plots show fairly constant modulation across the x-direction, but vertical line modulation is more dependent on postion than was the horizontal line modulation. Both green and red channels show similar trends. It is important that the green and red channel results be consistent because the ratio of these signals will be computed and used to identify blood vessel targets.

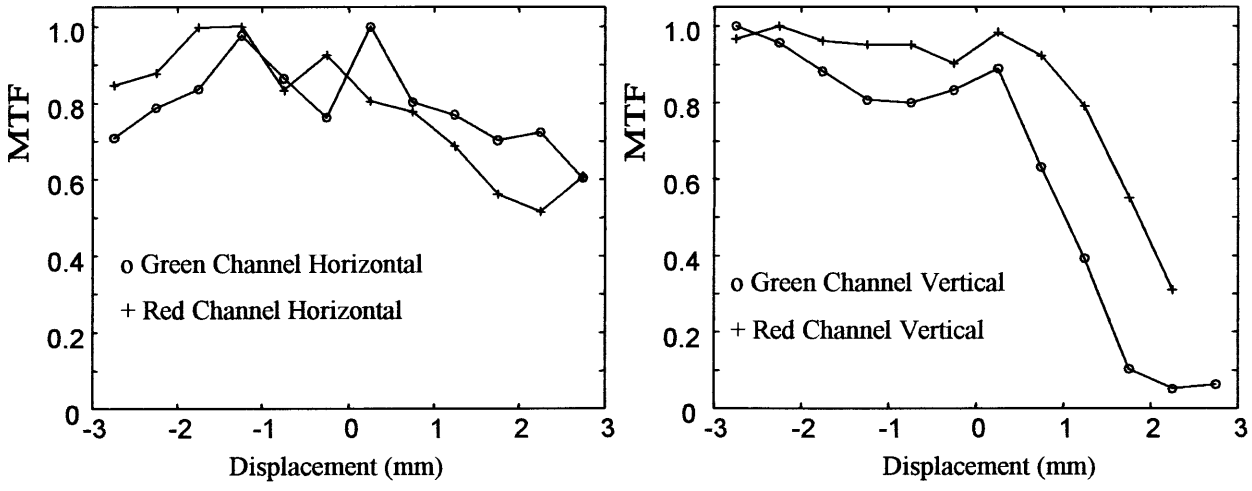

Figure 17: MTF of horizontal (left) and vertical (right) lines over changes in x (parallel to line scan.

The MTF versus y-position plot was generated by measuring the modulation changes associated with moving the 125 μm horizontal and vertical lines to different positions in the scanning field, perpendicular to the white light illumination (Figure 18). In the y-direction (perpendicular to the line illumination), treand similar to the x-displacement data are observed. Again, the MTF is fairly constant, and the red and green channels show similar trends. The vertical line MTF is again more sensitive to lateral position than the horizontal line modulation.

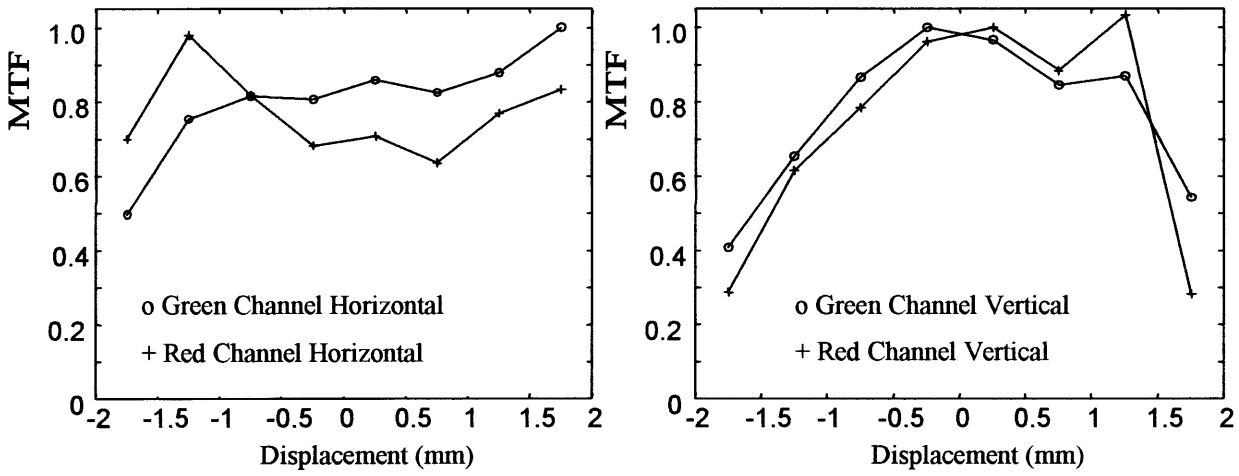

Figure 18: MTF of horizontal (left) and vertical (right) lines over changes in y

5.3.2 MTF versus axial position

Measurements were made to quantify the MTF versus axial position (Figure 19). The zero depth represents the closest distance the sample can physically be brought to the line illumination. Increasing depth corresponds to increased distance between the scanning system and the sample. Like the lateral displacement measurements, the green and red channels show similar trends and the modulations associated with the vertical lines are more sensitive to axial position than are modulations of horizontal lines. An important conclusion drawn from the measurements is that the imaging system is relatively insensitive to axial position across a great distance.

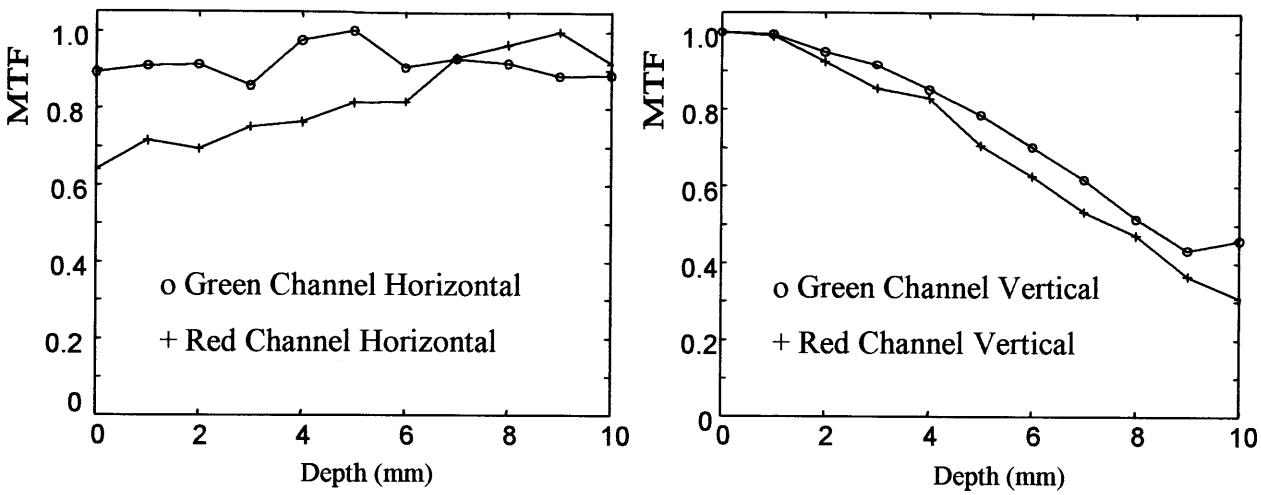

Figure 19: Modulation transfer function versus depth for horizontal (left) and vertical (right) lines.

Chapter Six

Closed Loop Control of Laser

6.1 Preliminary results with blood

Patterns of oxygenated human blood were created to mimic a blood vessel network in order to test the system's ability to image and identify blood vessel targets in a high contrast environment. Test pattern images were first acquired at 577 nm and 640 nm (Figure 20) after which the ratio image (577 nm/640 nm) was computed and dynamic range expanded. Next, the histogram of pixel values for this normalized image was graphed to identify the appropriate threshold for blood vessel targets. The 0.7 threshold was used to create the final binary image where pixel values less than 0.7 are assigned as black, representing blood vessels.

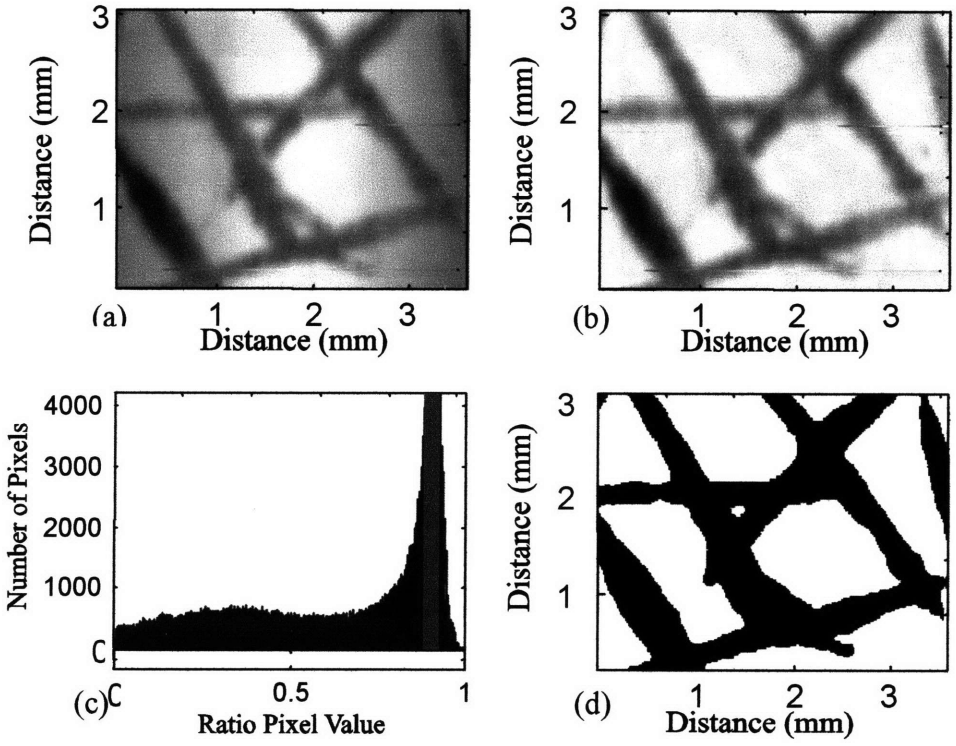

Figure 20: Succession of steps in identifying laser coordinates. Original 577 nm reflectance image (a), ratio normalized image (b), histogram of normalized image (c), and final image with laser coordinates represented as black using a 0.7 threshold (d).

Figure 21 illustrates two possible laser targeting strategies with the Smart Scalpel. The line scan image represents the PWS subregion to be treated, with blood vessels interspersed throughout the skin. The gray line represents the line of data acquired at a given instant, while the lighter gray circles are the laser targets. After determining blood vessel positions from a small number of line scans, a randomly selected subset of blood vessel targets are targeted for illumination with the heating laser beam (Figure 21a). However, to effectively heat the blood vessels, it may be important that the laser follow along one vessel at a time (Figure 21b), perhaps in the direction of the blood flow to maximize the efficiency of heat transfer to the blood vessels. Implementation of this targeting strategy will require a larger image to identify and track the spatial position of individual vessels.

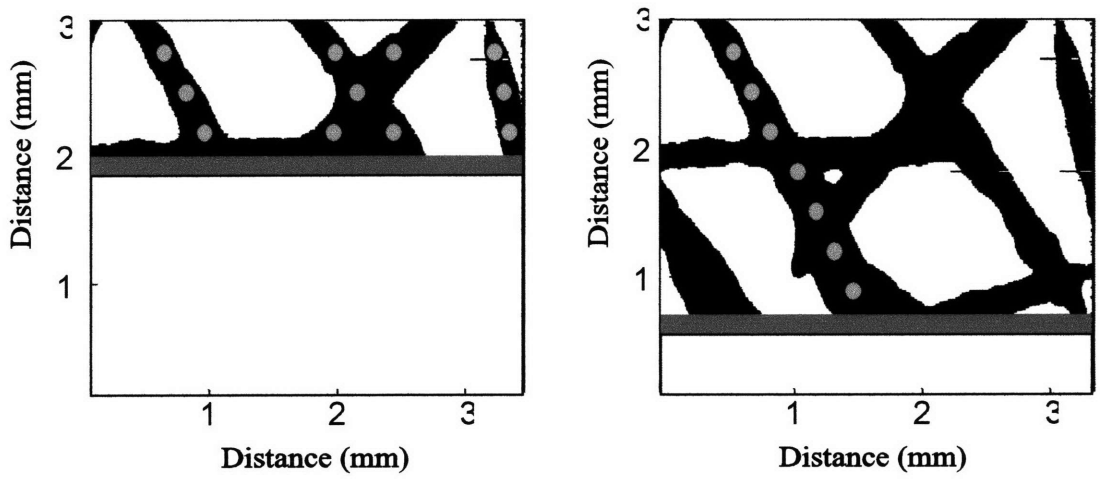

(a) (b)

Figure 21: Two possible control strategies to cover laser targets are illustrated. The first (a) covers one line at a time and delivers energy to the vessel locations within that line. The second (b) requires pattern recognition to identify continuous vessels and follow along one vessel at a time.

6.2 Simultaneous two-wavelength imaging to distinguish blood from other materials

Simultaneous two-wavelength imaging was used to distinguish blood from black ink on a test pattern (Figure 22). Lines of blood were painted on a white paper background. To test the ability of the system to identify blood, lines of black ink were drawn between the lines of blood. The first image (a) is from the green channel, which detects absorption of both blood and ink. Image (b) is the red channel image, which shows only the black ink absorbance. The image

created by ratioing the green and red sensor data (c) makes the blood regions more apparent and suppresses the pen ink. Finally, using a threshold cut-off of 0.95 on the ratio image, a binary image is generated with black areas representing targets for the laser-scanning subsystem.

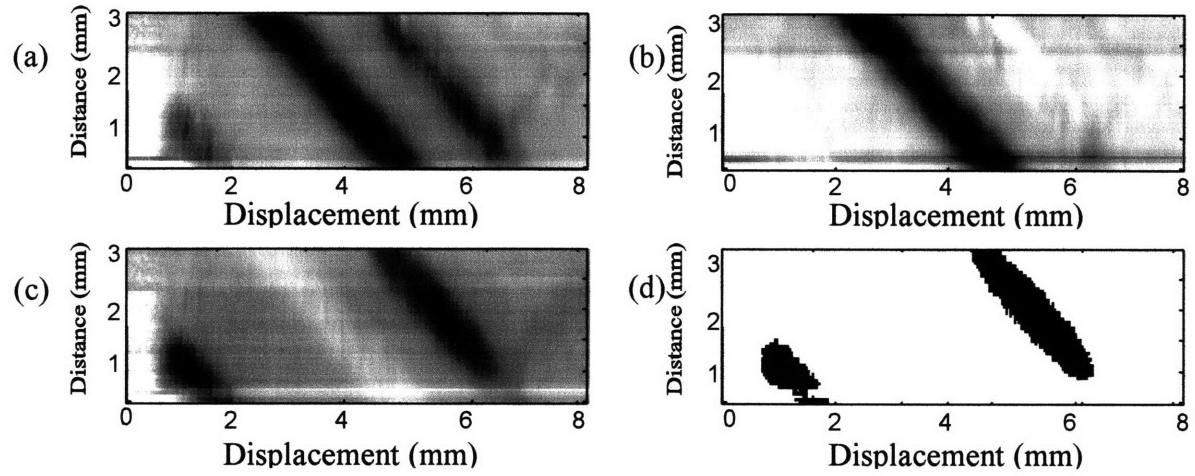

Figure 22: Steps in distinguishing blood from ink painted on white paper. (a) Green channel image, which shows absorbance of blood and ink. (b) Red channel shows only ink absorption. (c) Ratio image makes blood more apparent and suppresses ink signal. (d) Binary threshold image generated from ratio image to be used for laser targeting.

6.3 Fast closed loop control of laser

Fast closed loop imaging and laser targeting was tested using the same reticle discussed in previous sections. Images of the test reticle were acquired at rates of 25 lines/s on both, meaning the 50 line images shown in Figure 23 were acquired in 2 s. Once the 50 lines were acquired, the software program imported data previously acquired from a uniformly reflecting sample (mirror) to normalize the data. The ratio image with a threshold of 0.8 was used to generate the binary image shown in Figure 23(d). The black areas represent the targets that were then transferred to the beam scanning system.

The two random access galvanometers then scanned the beam across a two-dimensional field and the beam shutter modulated the laser energy. The shutter was open when the beam was in the position of a target and remained closed for all other locations. The entire imaging and laser scanning loop took approximately 5 s for the 50 line images. Image acquisition could be done ~4 times faster before reaching the 100 ksample/s limit of the Mirada data acquisition board. Laser scanning speeds are currently limited by the step-response of the galvanometers, ~5-10 ms.

However, if pattern recognition were incorporated into the software, the two random access galvanometers could identify the targets and follow these lines rather than cover the entire region.

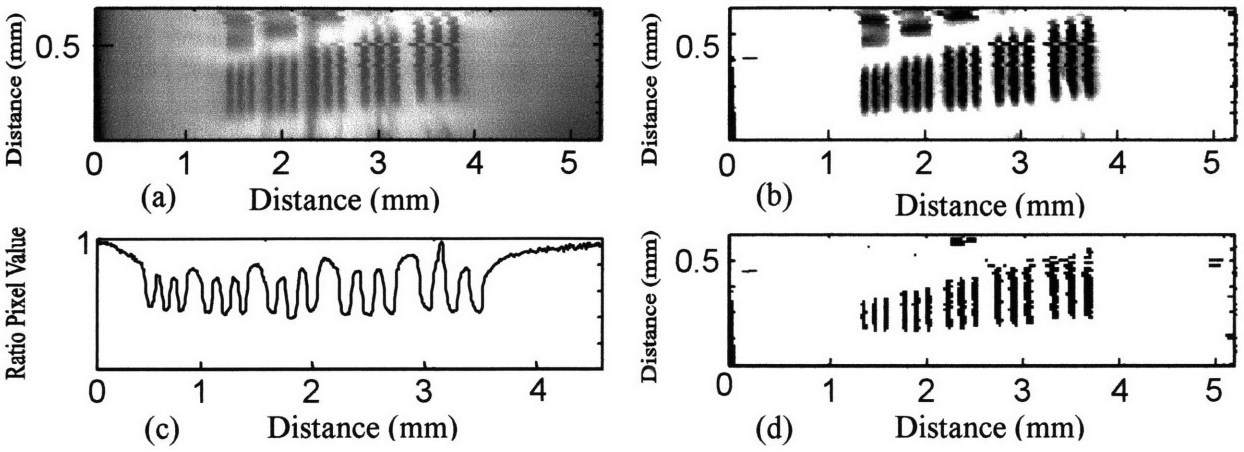

Figure 23: Steps in generating targets for the laser scanning system from a test reticle (a) Green channel image, (b) Ratio image using green channel data and previously acquired data from a uniform mirror reflection. (c) Ratio image makes blood more apparent and suppresses ink signal. (d) Binary threshold image (threshold = 0.8) generated from ratio image to be used for laser targeting.

Accuracy of laser scanning system was verified by imaging the laser pattern scanned on a white screen (Figure 24). As the laser continueously scanned the acquired pattern, a slow scan camera (using 4 s integration time) was used to image the laser light light pattern. These results agree well with the reticle image.

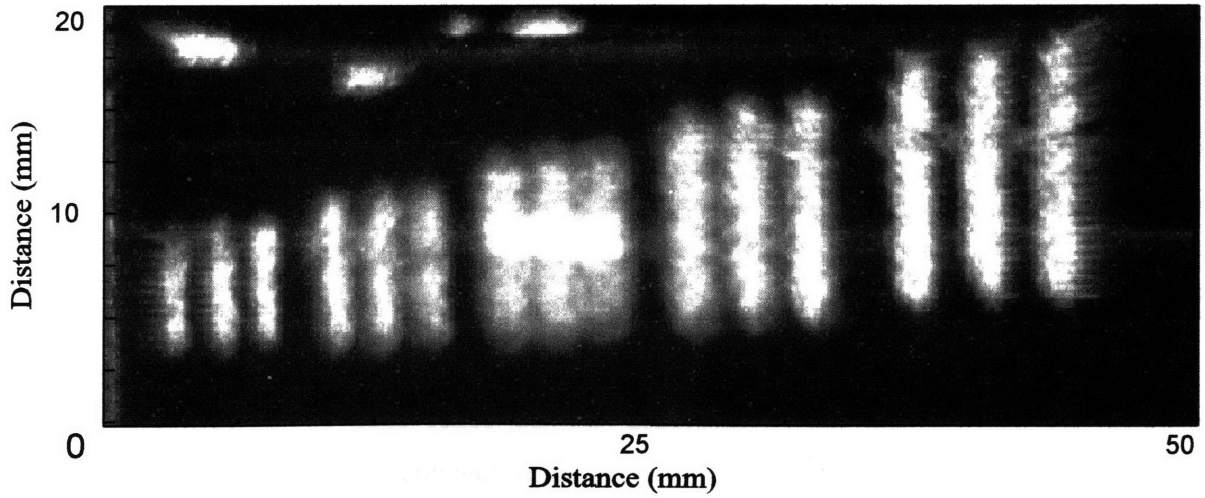

Figure 24: Pattern of light generated from reticle image and replicated by laser scanning system.

Chapter Seven

Other Potential Smart Scalpel Applications

7.1 Potential Smart Scalpel applications

Many other potential applications have been considered for the Smart Scalpel system, including automated identification and laser treatment of varicose veins, to reduce the tedious nature of the procedure. Another possibility is selective identification and treatment of cancerous tissue, since cancerous tissues are known to have unique spectroscopic properties that enable one to distinguish between tumors and normal tissue. We have also considered using of laser-induced fluorescence measurements to aid in identification of atherosclerotic plaque or use of fluorescence measurements to control dental drilling. One application, permanent or semi-permanent hair removal will be discussed in the following section.

7.2 Laser-assisted semi-permanent or permanent hair removal

7.2.1 Current clinical practice

Individuals with unwanted hair are prone to adverse psychological and cosmetic disturbances prompting them to seek medical advice. This has driven the development of methods for temporary hair removal, including shaving, wax epilation, and use of chemical depilatories [Kvedar, Gibson and Krusinski, 1985; Richards, Marguerite and Meharg, 1990]. Electrolysis is a well-established method for permanent destruction of terminal hair follicles. However, the method is tedious, and efficacy has been reported to be between 15% and 50% permanent hair loss [Wagner, 1990]. Scarring can result after electrolysis, especially if inexpertly performed [Kligman and Peters, 1984].

Laser-assisted hair removal methods [Wheeland, 1997] have been developed recently as a minimally invasive alternative approach to hair removal. Two general approaches have been identified so far. The first relies on the absorption properties of melanin, an intrinsic chromophore found in high concentration in follicles of pigmented hair. Hair follicles are damaged by selective photothermolysis [Anderson and Parish, 1983] when illuminated with light

at a wavelength absorbed by melanin. In one embodiment [Dierickx *et al.*, 1998], selective thermal injury to both superficial and deep portions of pigmented hair follicles was reported on illumination of the skin with a 3 ms light pulse at 694 nm from a ruby laser having an incident fluence level between 0.1 to 0.75 MJ/m^2. The treated area per laser shot is between 10 – 12 mm in diameter. Only 15% to 20% of the incident light penetrates through the dermis to the follicles; the remainder is dissipated in the dermis as heat. Consequently, an actively cooled glass sapphire prism/lens system is used to heat sink the skin to minimize thermal injury to the pigmented epidermis. There is a 2 to 6 month delay reported in hair regrowth after a single treatment for individuals with highly pigmented hair (brown or black).

The second general approach [Nanni and Alster, 1997; Goldberg, 1995] to laser-assisted hair removal utilizes long wavelength near infrared light (1064 nm) to increase the penetration of laser energy into the dermis. The low absorption of natural chromophores like melanin at the illumination wavelength is offset by introduction of an exogenous chromophore into the hair follicle to enhance light absorption by the hair follicle cells. Input of the laser energy into the dermis on a time scale much shorter than the follicle thermal relaxation time (<100 ns) results in selective damage of the follicle cells by excessive heat. However, the presence of a mechanical shock wave caused by the superheated fluid surrounding the particle or the fragmentation of the particle itself could also be responsible for causing mechanical damage to adjacent cells. Illumination of the treated area with light from a Q-switched neodymium:yttrium-aluminum garnet (Nd:YAG) laser (λ = 1064 nm, $\tau_p < 10$ ns, J = 20 to 30 kJ/cm^2) over a 7 mm spot size has resulted in a 3 to 6 month delay in hair regrowth.

A common element to both the endogenous and exogenous chromophore techniques described above is the reliance on selective absorption of laser radiation in the illuminated area to damage hair follicle cells. Because of the relatively small difference in absorption between targeted and adjacent cells, collateral damage can be significant resulting in pain and discomfort to the patient both during and after the procedure. Evidence for collateral damage to the dermis stems from reports of postoperative edema and erythema for periods of 24 – 48 hours after the hair removal treatments.

7.2.2 Smart Scalpel approach

One solution to this difficulty is implementation of a Smart Scalpel scheme in which the hair follicles are first identified by means of a spectroscopic measurement. A laser beam is then focused on the hair follicle to deliver a radiation dose sufficient to either destroy or inhibit the ability of follicle cells to grow hair. This approach could be implemented in a full-field or line scan imaging format or, as diagrammed in Figure 25, as a hand-held device (known as the "LaserShaver") manually scanned across the skin's surface. In this embodiment, a two-wavelength reflectance measurement identifies the presence of a hair follicle and generates a trigger to fire a laser to selectively heat cells in the hair follicle.

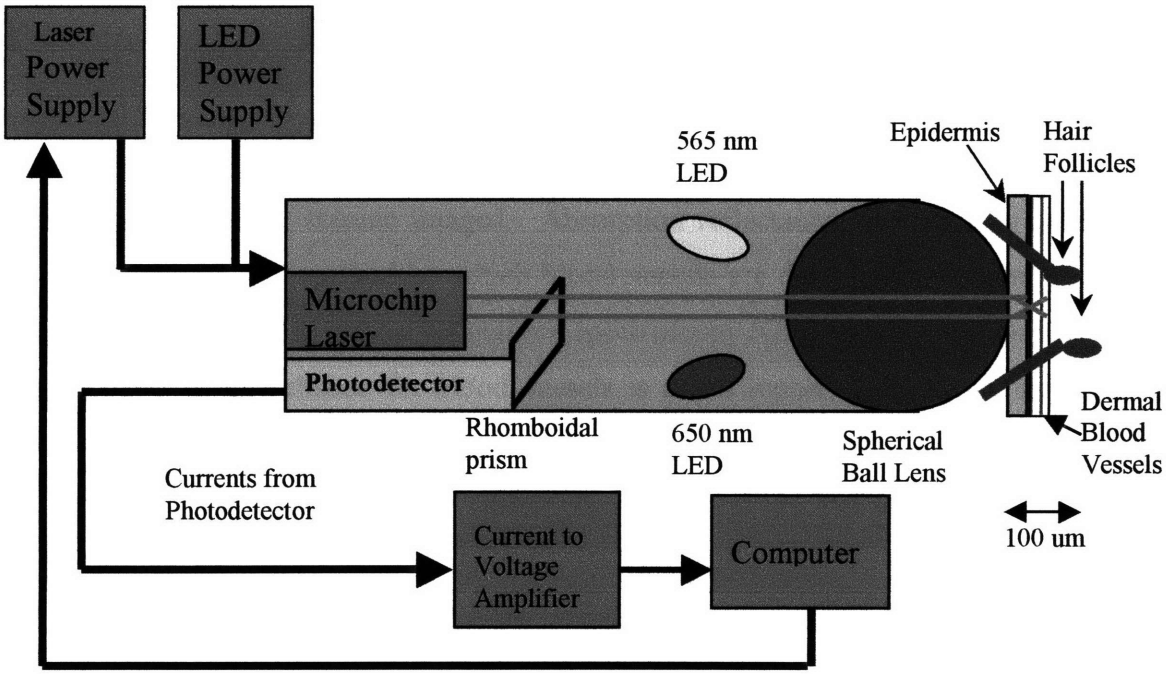

Figure 25: Schematic of miniaturized "LaserShaver".

Chapter Eight

Conclusions and Future Work

The Smart Scalpel represents a new class of medical instrument, which utilizes real-time information about tissue properties to selectively deliver therapeutic laser energy to the specific blood vessel targets of a PWS. The Smart Scalpel approach to PWS treatment requires, first, locating the blood vessels within a volume of PWS and, second, illuminating selected blood vessels with light from a focused laser beam for a time sufficient to increase the local vessel temperature to cause permanent physical damage.

Major design components of the PWS Smart Scalpel are (1) a non-invasive method to selectively identify and locate blood vessels within the PWS; (2) a means to deliver the heating laser energy to the appropriate spatial location for the required time and (3) a strategy for heating blood vessels within the PWS volume imaged. Absorption reflectance spectroscopy with polarized light is the non-invasive method by which blood vessels are discriminated from other tissue in the PWS. We have chosen optical reflectance spectroscopy (ORS) for the treatment of port wine stains because the absorbance for blood vessels is much higher than that of the surrounding tissue at the 577 nm wavelength. With ORS we may use a diffuse white light illumination of the port wine stain skin to detect the backscattered light at visible and near infrared wavelengths. We then filter this backscattered light to retrieve only the wavelengths of interest: one wavelength at a peak oxyhemoglobin absorbance, and a second outside the absorption band for normalization.

Effective heating of blood in a vessel requires absorption of optical energy by the blood in a vessel at a rate sufficient to overcome thermal losses and raise the local blood temperature to cause irreversible thermal damage. To achieve optimal opto-thermal coupling of radiation into a blood vessel, several criteria must be satisfied. First, the laser wavelength should coincide with one of the oxyhemoglobin absorption bands (415, 540, 577 or 940 nm) and, second, the laser light is focused to a diameter equal to the mean diameter of blood vessels in a typical PWS (ca. 50 μm).

Effective implementation of either laser targeting strategies demands minimal relative motion between the image area and the PWS during the image acquisition, processing and targeting sequence. Tremor is the major source of motion for which the Smart Scalpel must compensate. The 10 Hz tremor frequency requires that a region be imaged and treated within ~50 ms. Because of this concern over relative motion between the patient and instrument, a line imaging and point laser scanning approach has been selected. This method allows dynamic control of the size of the imaged and treated area to optimally treat PWS skin with different density of blood vessels and varying degrees of patient movement.

From these design specifications, a prototype Smart Scalpel instrument has been built with imaging and laser scanning capabilities, with a treatment area of ~6 mm by 8 mm and a resolution of ~50 μm. The modulation transfer functions have been measured for the system over a range of spatial frequencies and positions in a three dimensional space. These results show that modulation is quite uniform within the imaging plane and in the axial direction. A software program as been developed to acquire these images, perform the necessary ratio and threshold operations to identify targets, and then convert these targets to coordinates of a laser scanning system, which includes two random-access galvanometers and a beam modulator. This closed-loop system has been demonstrated to successfully identify and track movements ~100 μm bars on a test pattern and direct laser scanning to trace these bars. The system can also clearly distinguish blood from ink deposited on a white background.

8.1 Original Contributions

A real-time, closed-loop surgical instrument was designed and developed to identify and selectively target blood vessels in a PWS. Original contributions include optical system design and construction, quantification of imaging system resolution and contrast, and preliminary verification of the imaging and targeting strategies. These original contributions are evidenced in the following two publications from SPIE conference oral presentations:

Sebern, E.L., Brenan, C.J.H., Anderson, R.R. and Hunter, I.W. Laser treatment of port wine stains using spectroscopic feedback: the "smart scalpel." *SPIE Proceedings, Cutaneous Applications of Lasers: Dermatology, Plastic Surgery, and Tissue Welding*, 1999, **3590**.

Sebern, E.L., Brenan, C.J.H., Anderson, R.R. and Hunter, I.W. Tissue modification with feedback: the "smart scalpel." *SPIE Proceedings, Microrobotics and Manipulation*, 1998, **3519**, 62-69.

8.2 Future Work

There are several limitations to the present Smart Scalpel system that can be addressed to improve its operation. First, the signal generated by the photodectors in insufficient to reliably distinguish blood vessels from the surrounding tissue in a mouse ear. In the current system, white light line illumination of the mouse has insufficient brightness for the photodetectors (in short integration times required) to generate large enough voltage signals to effectively perform the ratio and threshold operations in the software. It seems that the fundamental problem in the current design is the incoherence of white light source. As the white light output from the rectangular bundle passes through the optical system the light diverges quite rapidly, resulting in substantial light loss by the time this line illumination reaches the skin surface. Ideas for improving this coupling include:

- Rigorous analysis of current lens system used to couple the white light illumination to the skin surface. Such analysis may identify the main causes of light loss. By modifying the optics, it may be possible to more efficiently transmit the line of light to the skin surface.

- Direct full-field illumination of the skin with a mask over the CCD line array to spatially filter the reflected signal, creating the desired resolution between lines.

- Replace the spatially incoherent white light source with two lasers to illuminate the skin. Possible laser sources for this illumination include: a frequency doubled Nd:YAG or a 577 nm dye laser for the oxyhemoglobin signal and a 632.8 helium-neon laser for the normalization wavelength. A fast resonant scanner can be used to generate lines of light

from the two laser beams, and a random access galvanometer scans this line illumination to the desired skin locations.

With this improved imaging contrast, efforts can then be made to test the Smart Scalpel using an animal model, such as the mouse ear, rabbit ear or hamster cheek pouch. These models can be used to test the ability of the system to identify appropriate laser targets, and also gain knowledge of optimal laser parameters, such as wavelength, fluence, pulse width, and focused beam diameter. In addition, testing different laser scanning strategies (e.g. tracing individual vessels or targeting blood vessels in random order), in animal models will help determine the optimal method to treat human PWS skin.

Once the blood vessel absorption signal is improved, efforts can be made to acquire skin images and direct the laser faster than the current hardware capabilities, to reduce the potential for relative motion between the instrument and the patient. Image acquisition in the current system is limited by maximum sampling rate (100 ksamples/s) of the A/Ds on the Mirada board. If the Mirada board is replaced with another data acquisition board with higher bandwidth or a frame grabber board, higher frame rates could be achieved. Assuming that the PCI bus on the computer is capable of sustained data rates of ~50 Mbytes/s, we can acquire lines at a rate of 25 lines/ms. It is also possible to bypass the computer in the ratio and threshold operation if a frame grabber board with these capabilities is selected. On the laser-scanning side, speed of laser targeting is limited by the step response of the General Scanning 350DT galvanometers (~5-10 ms). Galvanometers are currently being developed with shorter step responses, ~1 ms.

Once high contrast images can be obtained *in vivo*, and the imaging and laser scanning systems operate to treat an adequate-size area (~10 mm by 10 mm) within the period of tremor (~50 ms), the Smart Scalpel instrument can be modified for use in a clinical setting. Because the functional prototype is quite large, efforts must be made either to position the Smart Scalpel remote from the patient or to miniaturize the system. As a first step, a fiber bundle may be used to transmit the line illumination and heating laser to the patient, as well as relay the light reflected and backscattered from the patient to the photodetectors. In the longer term, the opto-mechanical system can be re-designed into a smaller format through the use of specialized lenses, scanners,

light sources, and photodetectors that make this miniaturization feasible. Finally, once the Smart Scalpel is demonstrated to be effective in the treatment of PWS, efforts can be made to apply the real-time, closed-loop approach to other medical procedures.

Appendix A- Smart Scalpel Software

```
/*************************************************************************
mirada_imaging.c
by Beth Sebern
Created on Sept. 8, 1998
Last modified on Apr. 25, 1999

A/D         Chan 7 = Start Pulse Input to Begin Data Acquisition (only for ImageAnalog function)
            Chan 5 = Clock Pulse Input to Synchronize Data Acquisition (only for ImageAnalog function)
            Chan 2 = Data for Green Array
            Chan 4 = Data for Red Array

D/A         Chan 0 = Control of Imaging Galvanometer
            Chan 1 = Control of Laser X-axis Galvanometer
            Chan 2 = Control of Laser Y-axis Galvanometer
            Chan 3 = Laser shutter control


DIN         Chan 0 = Start Pulse Input to Begin Data Acquisition (only for ImageDigital function)
            Chan 1 = Clock Pulse Input to Synchronize Data Acquisition (only for ImageDigital function)

A/D max voltage = 4.5 = 32767
D/A max voltage = 3.0 = 131071
/*************************************************************************
                                    INCLUDES
*************************************************************************/
#include <stdio.h>
#include <stdlib.h>
#include <conio.h>
#include <math.h>
#include <windows.h>
#include <winbase.h>
#include "userdll.h"
/*************************************************************************
                            GLOBAL DEFINITIONS AND VARIABLES
*************************************************************************/
#define DIO_OUT 18 // Mirada memory offset location (Currently not using the DOUT's)
#define DIO_IN 19          // Mirada memory offset location
#define numberOfLines 50   // Number of line array outputs per scan
```

```
volatile int *AtoDMem;        // Pointer to Mirada 1 memory location

double dt;                                  // Setting for clock resolution
int iGreenData[numberOfLines][1024];        // 2-D array for a single green line scan
int iRedData [numberOfLines][1024];                 // 2-D array for a single red line scan
double dRatioGreen [numberOfLines][1024];
double dRatioRed [numberOfLines][1024];
double dRatioTwoChannel [numberOfLines][1024];
int iSubtractGreen [numberOfLines][1024];
int iSubtractRed [numberOfLines][1024];
int iSubtractTwoChannel [numberOfLines][1024];
int iThresholdRed [numberOfLines][1024];
int iThresholdGreen [numberOfLines][1024];
int iThresholdTwoChannel [numberOfLines][1024];

int dinHigh1=1;               //start pulse high
int dinHigh2=2;               //clock pulse high
int dinHigh3=4;               //currently not used
int dinHigh4=8;               //currently not used
/*************************************************************************
                              FUNCTION PROTOTYPES
*************************************************************************/
void Timer(double dt);
void InitMirada1(void);
void ImageAnalog(void);
void ImageDigital(void);
void RatioRed(void);
void RatioGreen(void);
void RatioThresholdTwoChannel(void);
void SubtractRed(void);
void SubtractGreen(void);
void SubtractThresholdTwoChannel(void);
void LaserScan(void);
void CreateFiles(void);
/*************************************************************************
                              MAIN PROGRAM
*************************************************************************/
void main() {

        printf("Initializing Mirada board ...\n");              // Initialize Mirada Board
                if (ourdll_Init() != SUCCESS){
                        printf("Could not initialize driver.\nExiting.\n");
                        exit(1);
                }
        AtoDMem = ourdll_AtoDMem();
        printf("Done\n");
```

```
        dt=10e-6;                                   //has dt=10 usec
        Timer(dt);

        printf("Imaging in progress\n");
        printf("\n");
        printf("To stop, hit Ctrl-C ....\n");

        while(1){
        //ImageAnalog();
        ImageDigital();
        RatioRed();
        RatioGreen();
        RatioThresholdTwoChannel();
        CreateFiles();
        LaserScan();
        }

}

/*************************************************************************
        MIRADA IMAGING WHILE LOOP USING DIGITAL INPUTS TO TRIGGER
*************************************************************************/
void ImageDigital(void){

        int iStartPulseMonitor = 0;
        int iClockPulseMonitor = 0;
        int iStartPulseHigh=1;          //start pulse high (Din Channel 0)
        int iClockPulseHigh=2;          //clock pulse high (Din Channel 1)

        int m;

        int iGalvoVoltage1 = 7500;              // -0.17 V < iGalvoVoltage1 < 0.17 V
        int iGalvoVoltageMax1 = 7500;           //Max. 0.17 V
        int iGalvoStep1 = 50;                   //1.1 mV step

        int iLine = 0;
        int iGreenPixel = 0;
        int iRedPixel = 0;
        int iGreenPixelValue= 0;
        int iRedPixelValue = 0;

        RTSetPriority(3);                       //Gives highest priority to data acquisition
        *(volatile int *)(AtoDMem + 0)=iGalvoVoltage1;  // Write galvo voltage to channel 0
        for(m=0; m<1000; m++){                  // Delay 10 ms for settling time of galvo
                Timer(0.);
```

```
}

while(iLine<numberOfLines){
        *(volatile int *)(AtoDMem + 0)=iGalvoVoltage1; // Write to chan. 0 galvo
        for(m=0; m<100; m++){                   // Delay 1 ms for settling time of galvo
                Timer(0.);
        }

        do{
                iStartPulseMonitor=*(volatile short int *)(AtoDMem + DIO_IN);
        }
        while((iStartPulseMonitor &iStartPulseHigh) != iStartPulseHigh);
        while(iGreenPixel<1024){
                do{
                        iClockPulseMonitor=*(volatile short int *)(AtoDMem + DIO_IN);
                }
                while ((iClockPulseMonitor &iClockPulseHigh) != iClockPulseHigh);

                iGreenData[iLine][iGreenPixel]=*(volatile short int *)(AtoDMem + 2);

                do{
                        iClockPulseMonitor=*(volatile short int *)(AtoDMem + DIO_IN);
                }
                while ((iClockPulseMonitor &iClockPulseHigh) == iClockPulseHigh);
                iGreenPixel++;
        }

        do{
                iStartPulseMonitor=*(volatile short int *)(AtoDMem + DIO_IN);
        }
        while((iStartPulseMonitor &iStartPulseHigh) != iStartPulseHigh);

        do{
                iClockPulseMonitor=*(volatile short int *)(AtoDMem + DIO_IN);
}
        while ((iClockPulseMonitor &iClockPulseHigh) != iClockPulseHigh);

        do{
                iClockPulseMonitor=*(volatile short int *)(AtoDMem + DIO_IN);
}
        while ((iClockPulseMonitor &iClockPulseHigh) == iClockPulseHigh);

        while(iRedPixel<1024){
                do{
                        iClockPulseMonitor=*(volatile short int *)(AtoDMem + DIO_IN);
                }
```

```
                while ((iClockPulseMonitor &iClockPulseHigh) != iClockPulseHigh);

                iRedData[iLine][iRedPixel]=*(volatile short int *)(AtoDMem + 4);

                do{
                        iClockPulseMonitor=*(volatile short int *)(AtoDMem + DIO_IN);
                }
                while ((iClockPulseMonitor &iClockPulseHigh) == iClockPulseHigh);
                iRedPixel++;
        }
        iLine++;
        iGalvoVoltage1 = iGalvoVoltage1+iGalvoStep1;
        iGreenPixel=0;
        iRedPixel=0;
    }

    *(volatile int *)(AtoDMem + 0)=0;

    RTSetPriority(1);                       //Sets program priority back to normal
}

/*****************************************************************************
                        RATIO AND THRESHOLD OPERATIONS
*****************************************************************************/
void RatioGreen(void){

    FILE *fptMirrorImageGreen;
    FILE *fptCopyOfFile;

    int iLine = 0;
    int iMirrorPixel = 0;
    int iRatioPixel = 0;
    int iThresholdPixel = 0;
    int mirrorGreen = 0;
    int newArrayGreen[numberOfLines][1024];
    double dCutoffGreen = .7;    // Arbitrary threshold set to discriminate blood vessels

    fptMirrorImageGreen = fopen("existing_file_green.dat", "r");
    for (iLine=0;iLine<numberOfLines;iLine++){              // Import Mirror File
        for (iRatioPixel=0;iRatioPixel<1024;iRatioPixel++){
            fscanf(fptMirrorImageGreen, "%i", &mirrorGreen);
            newArrayGreen[iLine][iRatioPixel]=mirrorGreen;
        }
    }
    fclose(fptMirrorImageGreen);
```

```
	for (iLine=0;iLine<numberOfLines;iLine++)
		for (iRatioPixel=0;iRatioPixel<1024;iRatioPixel++){
			if(newArrayGreen[iLine][iRatioPixel] <= 0)
				newArrayGreen[iLine][iRatioPixel]=1;
			else

	newArrayGreen[iLine][iRatioPixel]=newArrayGreen[iLine][iRatioPixel];
	dRatioGreen[iLine][iRatioPixel]=(double)iGreenData[iLine][iRatioPixel]/(double)newAr
rayGreen[iLine][iRatioPixel];
		}
	}
}

void RatioRed(void){

	FILE *fptMirrorImageRed;

	int iLine = 0;
	int iMirrorPixel = 0;
	int iRatioPixel = 0;
	int iThresholdPixel = 0;
	int mirrorRed = 0;
	int newArrayRed[numberOfLines][1024];
	double dCutoffRed = .7;	// Arbitrary threshold set to discriminate blood vessels

	fptMirrorImageRed = fopen("existing_file_red.dat", "r");
	for (iLine=0;iLine<numberOfLines;iLine++){		// Import Mirror File
		for (iRatioPixel=0;iRatioPixel<1024;iRatioPixel++){
			fscanf(fptMirrorImageRed, "%i", &mirrorRed);
			newArrayRed[iLine][iRatioPixel]=mirrorRed;
		}
	}
	fclose(fptMirrorImageRed);

	for (iLine=0;iLine<numberOfLines;iLine++){
	for (iRatioPixel=0;iRatioPixel<1024;iRatioPixel++){
			if(newArrayRed[iLine][iRatioPixel] <= 0)
				newArrayRed[iLine][iRatioPixel]=1;
			else

	newArrayRed[iLine][iRatioPixel]=newArrayRed[iLine][iRatioPixel];
		dRatioRed[iLine][iRatioPixel]=(double)iRedData[iLine][iRatioPixel]/(double)ne
wArrayRed[iLine][iRatioPixel];
		}
	}
}
```

```
void RatioThresholdTwoChannel(void){

	int iLine = 0;
	int iRatioPixel = 0;
	int iThresholdPixel = 0;
	double dCutoffTwoChannel= 0.95;

	for (iLine=0;iLine<numberOfLines;iLine++){		// Ratio of two channels
		for (iRatioPixel=0;iRatioPixel<1024;iRatioPixel++){
		dRatioTwoChannel[iLine][iThresholdPixel]=dRatioGreen[iLine][iRatioPixel]/dR
	atioRed[iLine][iRatioPixel];
			if(dRatioTwoChannel[iLine][iRatioPixel]>=dCutoffTwoChannel)
				iThresholdTwoChannel[iLine][iRatioPixel]=1;	//Thresholding
			else
				iThresholdTwoChannel[iLine][iRatioPixel]=0;
		}
	}
}
/*****************************************************************************
			SUBTRACTION AND THRESHOLD OPERATIONS
*****************************************************************************/
void SubtractGreen(void){

	FILE *fptMirrorImageGreen;
	FILE *fptCopyOfFile;

	int iLine = 0;
	int iMirrorPixel = 0;
	int iSubtractPixel = 0;
	int iThresholdPixel = 0;
	int mirrorGreen = 0;
	int newArrayGreen[numberOfLines][1024];
	int iCutoffGreen = 1000;	// Arbitrary threshold set to discriminate blood vessels

	fptMirrorImageGreen = fopen("existing_file_green.dat", "r");
	for (iLine=0;iLine<numberOfLines;iLine++){		// Import Mirror File
		for (iSubtractPixel=0;iSubtractPixel<1024;iSubtractPixel++){
			fscanf(fptMirrorImageGreen, "%i", &mirrorGreen);
			newArrayGreen[iLine][iSubtractPixel]=mirrorGreen;
		}
	}
	fclose(fptMirrorImageGreen);

	for (iLine=0;iLine<numberOfLines;iLine++){
		for (iSubtractPixel=0;iSubtractPixel<1024;iSubtractPixel++){
```

```
                if(newArrayGreen[iLine][iSubtractPixel] <= 0)
                        newArrayGreen[iLine][iSubtractPixel]=1;
                else
                newArrayGreen[iLine][iSubtractPixel]=newArrayGreen[iLine][iSubtractPixel];
        iSubtractGreen[iLine][iSubtractPixel]=iGreenData[iLine][iSubtractPixel]-
newArrayGreen[iLine][iSubtractPixel];
                }
        }
}

void SubtractRed(void){

        FILE *fptMirrorImageRed;

        int iLine = 0;
        int iMirrorPixel = 0;
        int iSubtractPixel = 0;
        int iThresholdPixel = 0;
        int mirrorRed = 0;
        int newArrayRed[numberOfLines][1024];
        int iCutoffRed = 1000;                  // Arbitrary threshold set to discriminate blood
vessels

        fptMirrorImageRed = fopen("existing_file_red.dat", "r");
        for (iLine=0;iLine<numberOfLines;iLine++){                      // Import Mirror File
                for (iSubtractPixel=0;iSubtractPixel<1024;iSubtractPixel++){
                        fscanf(fptMirrorImageRed, "%i", &mirrorRed);
                        newArrayRed[iLine][iSubtractPixel]=mirrorRed;
                }
        }
        fclose(fptMirrorImageRed);

        for (iLine=0;iLine<numberOfLines;iLine++){
                for (iSubtractPixel=0;iSubtractPixel<1024;iSubtractPixel++){
                        if(newArrayRed[iLine][iSubtractPixel] <= 0)
                                newArrayRed[iLine][iSubtractPixel]=1;
                        else
                newArrayRed[iLine][iSubtractPixel]=newArrayRed[iLine][iSubtractPixel];
                iSubtractRed[iLine][iSubtractPixel]=iRedData[iLine][iSubtractPixel]-
newArrayRed[iLine][iSubtractPixel];
                }
        }
}

void SubtractThresholdTwoChannel(void){
```

```
        int iLine = 0;
        int iSubtractPixel = 0;
        int iThresholdPixel = 0;
        double iCutoffTwoChannel= 1000;

        for (iLine=0;iLine<numberOfLines;iLine++){        // Ratio of two channels then
thresholding
                for (iSubtractPixel=0;iSubtractPixel<1024;iSubtractPixel++){
                iSubtractTwoChannel[iLine][iSubtractPixel]                              =
iSubtractGreen[iLine][iSubtractPixel]+iSubtractRed[iLine][iSubtractPixel];
                        if(iSubtractTwoChannel[iLine][iSubtractPixel]>=iCutoffTwoChannel)
                                iThresholdTwoChannel[iLine][iSubtractPixel]=1;
                        else
                                iThresholdTwoChannel[iLine][iSubtractPixel]=0;
                }
        }
}

}


/*************************************************************************
                        LASER SCANNING USING THRESHOLD DATA
*************************************************************************/

void LaserScan(void){

        int m;

        int iGalvoVoltageMinX = -19456;   //min= -0.4 V X-axis laser scanner (large paddle)
        int iGalvoVoltageMeanX = 0;               //mean = 0 V
        int iGalvoVoltageMaxX = 19456;    //mean = 0.4 V

        int iGalvoVoltageMinY = -14400;   //min= -0.3 V [Y-axis laser scanner (small paddle)]
        int iGalvoVoltageMeanY = 0;               //mean = 0 V
        int iGalvoVoltageMaxY = 14400;    //max = 0.3 V

        int iXcountsPerPixel = 38;                //Counts per pixel
        int iYcountsPerLine = 288;                //Counts per line (assuming 100 lines)

        int iShutterClosed = 26214;               //0.6 V for min. laser output
        int iShutterOpen = 13107;                 //0.3 V for max. laser output

        int iLine=0;
        int iPixel=0;
```

```
        *(volatile int *)(AtoDMem + 1)=iGalvoVoltageMinX;              //X-axis        control
channel
        *(volatile int *)(AtoDMem + 2)=iGalvoVoltageMinY;              //Y-axis        control
channel
        *(volatile int *)(AtoDMem + 3)=iShutterClosed;          //Laser shutter control channel

        for(iLine=1; iLine<=numberOfLines; iLine++){
                *(volatile int *)(AtoDMem + 2)=iGalvoVoltageMinY+(iYcountsPerLine*iLine);
                for(iPixel=1; iPixel<=1024; iPixel++){
                *(volatile int *)(AtoDMem +1)=iGalvoVoltageMinX+(iXcountsPerPixel*iPixel);
                        if(iThresholdTwoChannel[iLine][iPixel]==1)
                                *(volatile int *)(AtoDMem + 3)=iShutterOpen;
                        else
                                *(volatile int *)(AtoDMem + 3)=iShutterClosed;
                        for(m=0; m<5; m++){         //Delay 50 us to see scan
                                Timer(0.);
                        }
                }
        }
}

/*************************************************************************
                                WRITING DATA TO FILES
*************************************************************************/
void CreateFiles(void){

        FILE *fptGreen;
        FILE *fptRed;
        FILE *fptRatio;
        FILE *fptThreshold;
        int iLine;
        int iGreenPixel;
        int iRedPixel;
        int iRatioPixel;
        int iThresholdPixel;

        fptGreen = fopen("green.dat", "w");
        for (iLine=0;iLine<numberOfLines;iLine++){
                for (iGreenPixel=0;iGreenPixel<1024;iGreenPixel++){
                fprintf(fptGreen, "%i\n", iGreenData[iLine][iGreenPixel]);
                }
        }
        fclose(fptGreen);

        fptRed = fopen("red.dat", "w");
        for (iLine=0;iLine<numberOfLines;iLine++){
```

```
            for (iRedPixel=0;iRedPixel<1024;iRedPixel++){
            fprintf(fptRed, "%i\n", iRedData[iLine][iRedPixel]);
            }
        }
        fclose(fptRed);

        fptRatio = fopen("ratio.dat", "w");
        for (iLine=0;iLine<numberOfLines;iLine++){
            for (iRatioPixel=0;iRatioPixel<1024;iRatioPixel++){
            fprintf(fptRatio, "%f\n", dRatioTwoChannel[iLine][iRatioPixel]);
            }
        }
        fclose(fptRatio);

        fptThreshold = fopen("threshold.dat", "w");
        for (iLine=0;iLine<numberOfLines;iLine++){
            for (iThresholdPixel=0;iThresholdPixel<1024;iThresholdPixel++){
            fprintf(fptThreshold, "%i\n", iThresholdTwoChannel[iLine][iThresholdPixel]);
            }
        }
        fclose(fptThreshold);

}

/*************************************************************************
                    IMAGE ACQUISITION WITH ANALOG TRIGGER
*************************************************************************/
void ImageAnalog(void){
        int m;

        int iStartPulseMonitor = 0;
        int iStartPulseHigh = 16384;            //2.25 V threshold
        int iClockPulseMonitor = 0;
        int iClockPulseHigh = 16384;            //2.25 V threshold
        int iPulseLow = 0;

        int iGalvoVoltage1 = 2500;              // -0.17 V < iGalvoVoltage1 < 0.17 V
        int iGalvoVoltageMax1 = 7500;           //Max. 0.17 V
        int iGalvoStep1 = 50;                   //1.1 mV step

        int iLine = 0;
        int iGreenPixel = 0;
        int iRedPixel = 0;
        int iGreenPixelValue= 0;
        int iRedPixelValue = 0;
```

```
*(volatile int *)(AtoDMem + 0)=iGalvoVoltage1;   // Write galvo voltage to channel 0
for(m=0; m<1000; m++){                          // Delay 10 ms for settling time of galvo
        Timer(0.);
}

while(iLine<numberOfLines){
        *(volatile int *)(AtoDMem + 0)=iGalvoVoltage1;   // Write to chan. 0 galvo
        for(m=0; m<100; m++){                   // Delay 1 ms for settling time of galvo
                Timer(0.);
        }

        do{
                iStartPulseMonitor=*(volatile short int *)(AtoDMem + 7);
        }
        while (iStartPulseMonitor <= iStartPulseHigh);

        for(m=0; m<10; m++){  //100 usec Delay to get past the 2.5 usec clock pulse
delay
                Timer(0.);
        }

        while(iGreenPixel<1024){
                do{
                        iClockPulseMonitor=*(volatile short int *)(AtoDMem + 5);
                }
                while (iClockPulseMonitor <= iClockPulseHigh);

                for(m=0; m<10; m++){
                        Timer(0.);
                }
                iGreenData[iLine][iGreenPixel]=*(volatile short int *)(AtoDMem + 2);
                for(m=0; m<30; m++){                    // Delay 300 us for next clock pulse
before resampling
                        Timer(0.);
                }
                iGreenPixel++;
        }

        do{
                iStartPulseMonitor=*(volatile short int *)(AtoDMem + 7);
        }
        while (iStartPulseMonitor <= iStartPulseHigh);

        for(m=0; m<60; m++){
                Timer(0.);
        }
```

```
            while(iRedPixel<1024){
                do{
                    iClockPulseMonitor=*(volatile short int *)(AtoDMem + 5);
                }
                while (iClockPulseMonitor <= iClockPulseHigh);

                for(m=0; m<10; m++){
                    Timer(0.);
                }
                iRedData[iLine][iRedPixel]=*(volatile short int *)(AtoDMem + 4);
                for(m=0; m<30; m++){                // Delay 300 us for next clock pulse
before resampling
                    Timer(0.);
                }
                iRedPixel++;
            }

            iLine++;
            iGalvoVoltage1 = iGalvoVoltage1+iGalvoStep1;
            iGreenPixel=0;
            iRedPixel=0;
        }

        *(volatile int *)(AtoDMem + 0)=0;
}
```

References

Anderson, R.R. Laser medicine in dermatology, *The Journal of Dermatology*, 1996, **23**, 778-782.

Anderson, R.R Polarized light examination and photography of the skin, *Archives of Dermatology*, 1991, **127(7)**, 1000-1005.

Anderson, R.R. and Parish, J.A. Selective photothermolysis: precise microsurgery by selective absorption of pulsed radiation. *Science*, 1983, **220**, 524-527.

Anderson, R.R. and Parrish, J.A. The optics of human skin, *Journal of Investigative Dermatology*,1981, **77(1)**, 13-19.

Anvari, B., Tanenbaum, B.S., Hoffman, W., Said, S., Milner, T.E., Liaw, L.H. and Nelson, J.S. Nd:YAG laser irradiation in conjunction with cryogen spray cooling induces deep and spatially selective photocoagulation in animal models, *Physics in Medicine and Biology*, 1997, **42(2),** 265-82.

Barsky, S.H., Rosen, S., Geer, D.E. and Noe, J.M. The nature and evolution of port wine stains: a computer-assisted study, *Journal of Investigative Dermatology*, 1980, **74(3),** 154-7.

Chambers, I.R., Clark, D. and Bainbridge, C. Automation of laser treatment or port-wine stains. *Physics in Medicine and Biology*, 1990, **7**, 1025-1028.

Cheong, W.F., Prahl, S.A. and Welch, A.J. A review of the optical properties of biological tissues, *IEEE Journal of Quantum Electronics*, 1990, **26(12),** 2166-2185.

Dierickx, C.C., Grossman, M.C., Farinelli, W.A. and Anderson, R.R. Permanent hair removal by normal-mode ruby laser. *Arch. Dermatol.*, 1998, **134**, 837-842.

Dorf, R.C. and Bishop, R.H. *Modern Control Systems*, Addison-Wesley, Reading, MA, 1995.

Elble, AR.J. and Koller, W.C. *Tremor*, The Johns Hopkins University Press, Baltimore, 1979, 37-40.

Fiskerstrand, E.J., Svaasand, L.O., Kopstad, G., Dalaker, M., Norvang, L.T. and Volden, G. Laser treatment of port wine stains: therapeutic outcome in relation to morphological parameters, *British Journal of Dermatology*, 1997, **136(3),** 467-8.

Goodman, J. *An Introduction to Fourier Optics*. New York: McGraw-Hill, 1982.

Goldberg, D.J. Topical solution-assisted laser hair removal. *Lasers Surg. Med.*, 1995, **7S(47),** Abstract.

Inderfurth, J.H.C., Ferguson, R.D., Frish, M.B. and Birngruber, R. Dynamic reflectometer for control of laser photocoagulation on the retina. *Lasers in Surgery and Medicine*, 1994, **15**, 54-61.

Inoue, S. Foundations of confocal scanned imaging in light microscopy. *Handbook of Biological Confocal Microscopy, Second Edition*, Editor Pawley, J.B., New York: Plenum Press, 1995.

Jacques, S.L. and Prahl, S.A. Modeling optical and thermal distributions in tissue during laser irradiation. *Lasers in Surgery and Medicine*, 1987, **6**, 494-503.

Kimel, S., Svaasand, L.O., Hammer-Wilson, M., Schell, M.J., Milner, T.E., Nelson, J.S. and Berns, M.W. Differential vascular response to laser photothermolysis. *Journal of Investigative Dermatology*, 1994, **5**, 693-700.

Kligman, A.M. and Peters, L. Histologic changes of human hair follicles after electrolysis: a comparison of 2 methods. *Cutis.* 1984, **34**, 169-176.

Kvedar, J.C., Gibson, M. and Krusinski, P.A. Hirsutism: evaluation and treatment. *J Am. Acad. Dermatol.*, 1985, **12**, 215-225.

Laffitte, F., Mordon, S., Chavoin, J.P., Bonafe, J.L., Rouge, D. and Costagliola, M. Frequency-doubled Nd:YAG laser with automatic scanning in the treatment of PWS: preliminary report. *Lasers in Medicine and Science*, 1992, **7(3),** 341-350.

McDaniel, D.H. and Mordon, S. Hexascan: A new robotized scanning laser handpiece. *Cutis*, 1990, **45**, 300-305.

McKenzie, A.L. Physics of thermal processes in laser-tissue interactions, *Phys. Med. Biol.*, 1990, **35(9),** 1175-1209.

Mordon, S., Rotteleur, G., Brunetaud, J.M. and Apfelberg, D.B. Rationale for automatic scanners in laser treatment of port wine stains. *Lasers in Surgery and Medicine*, 1993, **13**, 113-123.

Mulliken, J.B., and Young, A.R. *Vascular Birthmarks- Hemangiomas and Malformations*, Saunders, Philadelphia, PA, 1988.

Nanni, C. and Alster, T.S. Optimizing treatment parameters for hair removal using a topical carbon-based solution and 1064-nm Q-switched Neodymium:YAG laser energy. *Arch. Dermatol.*, 1997, 1546-1549.

Nelson, J.S., Milner, T.E., Anvari, B., Tanenbaum, B.S., Kimel, S., Svaasand, L.O. and Jacques, S.L. Dynamic epidermal cooling during pulsed laser treatment of port-wine-stain. A new methodology with preliminary clinical evaluation, *Archives of Dermatology*, 1995, **131(6)**, 695-700.

Reinisch, L., Mendenhall, M.H. and Ossoff, R.H. Precise laser incisions, corrected for patient respiration with an intelligent aiming system. *Lasers in Surgery and Medicine*, 1997, **20**, 210-215.

Richards, R.N., Marguerite U. and Meharg, G. Temporary hair removal in patients with hirsutism: a clinical study. *Cutis.* 1990, **45**, 199-202.

Smithies, D.J., Butler, P.H., Pickering, J.W. and Walker, E.P. A computer controlled scanner for the laser treatment of vascular lesions and hyperpigmentation. *Clin Phys Physiol Meas*, 1991, **12(3),** 261-267.

Stewart, R.B., Benbrahim, A., LaMuraglia, G.M., Rosenberg, M., L'Italien, G.J., Abbott, W.M. and Kung, R.T.V. Laser assisted vascular welding with real time temperature control. *Lasers in Surgery and Medicine*, 1996, **19**, 9-16.

Tope, W.D. Personal communication. *SPIE International Biomedical Optics Symposium*, San Jose, CA, 1999.

Torres, J.H., Anvari, B., Tanenbaum, B.S., Milner, T.E., Yu, J.C. and Nelson, J.S. Internal Temperature Measurement in Response to Cryogen Spray Cooling of a Skin Phantom, *Proceedings of SPIE International Biomedical Optics Symposium*, San Jose, CA, 1999.

van Gemert, M.J.C., de Kleijn, W.J.A. and Hulsbergen Henning, J.P. Temperature behavior of a model port-wine stain during argon laser coagulation. *Physics in Medicine and Biology*, 1982, **27(9)**,1089-1104.

Wagner, R.F. Physical methods for the management of hirsutism. *Cutis.* 1990, **45**, 19-26.

Watts, K.P., Fairchild, R.G., Slatkin, D.N., Greenberg, D., Packer, S., Atkins, H.L. and Hannon, S.J. Melanin content of hamster tissues, human tissues, and various melanomas, *Cancer Research*, 1981, **41**, 467-472.

Wheeland, R.G. Laser-assisted hair removal. *Lasers in Dermatology*, 1997, **15**, 469-477.

Whelan, W.M. and Wyman, D.R. Investigations of large vessel cooling during interstitial laser heating. *Medical Physics*, 1995, **22(1)**, 105-115.